FEB 10 1997

NAS1.29/3-2:97-01

NASA Tech Briefs

National Aeronautics and
Space Administration

Electronic Components and Circuits

Electronic Systems

Physical Sciences

CONTIN

Materials

Computer Programs

Mechanics

Machinery

Fabrication Technology

Mathematics and Information Sciences

Life Sciences

97-01

January 1997

Ger 0830-L-02 97-01263

INTRODUCTION

Tech Briefs are short announcements of new technology derived from the research and development activities of the National Aeronautics and Space Administration. These Briefs emphasize information considered likely to be transferable across industrial, regional, or disciplinary lines and are issued to encourage commercial application.

Availability of NASA Tech Briefs and TSP's

Distribution of NASA Tech Briefs, a monthly periodical publication, is limited to engineers in U.S. Industry and to other domestic technology transfer agents. Requests for individual Tech Briefs or for Technical Support Packages (TSP's) announced herein should be addressed to

NASA Center for AeroSpace Information
Technology Transfer Office
800 Elkridge Landing Rd.
Linthicum Heights, MD 21090-2934
Telephone No. (301) 621-0245

Please reference the three-letter, five-digit control number located at the end of each Tech Brief. Information on NASA's Technology Utilization Program, its documents, and services is also available at the same facility.

Technology Utilization Officers and Patent Counsels are located at NASA field installations to provide technology-transfer access to industrial users. Inquiries can be made by writing to NASA field installations listed below.

Technology Utilization Officers and Patent Counsels

Ames Research Center
Technology Utilization Officer
Mail Code 223-3
Moffett Field, CA 94035

Patent Counsel
Mail Code 200-11
Moffett Field, CA 94035

Goddard Space Flight Center
Technology Utilization Officer
Mail Code 702-1
Greenbelt, MD 20771

Patent Counsel
Mail Code 204
Greenbelt, MD 20771

Lyndon B. Johnson Space Center
Technology Utilization Officer
Mail Code IC-4
Houston, TX 77058

Patent Counsel
Mail Code AL3
Houston, TX 77058

John F. Kennedy Space Center
Technology Utilization Officer
Mail Stop PT-PMO-A
Kennedy Space Center, FL 32899

Patent Counsel
Mail Code PT-PAT
Kennedy Space Center, FL 32899

Langley Research Center
Technology Utilization Officer
Mail Stop 143
Hampton, VA 23665

Patent Counsel
Mail Code 279
Hampton, VA 23665

Lewis Research Center
Technology Utilization Officer
Mail Stop 7-3
21000 Brookpark Road
Cleveland, OH 44135

Patent Counsel
Mail Code LE-LAW
21000 Brookpark Road
Cleveland, OH 44135

Jet Propulsion Laboratory
Technology Utilization Officer
Mail Stop 156-211
4800 Oak Grove Drive
Pasadena, CA 91109

NASA Resident Office-JPL
Technology Utilization Officer
Mail Stop 180-801
4800 Oak Grove Drive
Pasadena, CA 91109

Patent Counsel
Mail Code 180-801
4800 Oak Grove Drive
Pasadena, CA 91109

George C. Marshall Space Flight Center
Technology Utilization Officer
Code AT01
Marshall Space Flight Center, AL 35812

Patent Counsel
Mail Code CC01
Marshall Space Flight Center, AL 35812

John C. Stennis Space Center
Technology Utilization Officer
Code HA-30
Stennis Space Center, MS 39529

NASA Headquarters
Technology Utilization Officer
Code CU
Washington, DC 20546

Assistant General Counsel for Patent Matters
Code GP
Washington, DC 20546

Dryden Flight Research Center
Technology Utilization Officer
M/S D21-31
Bldg. 4832 Whse 7
Lilly Dr.
Edwards, CA 93523

BLANK PAGE

NASA TechBriefs

National Aeronautics and
Space Administration

January 1997
97-01

5 Electronic Components and Circuits

19 Electronic Systems

27 Physical Sciences

31 Materials

37 Computer Programs

41 Mechanics

47 Machinery

55 Fabrication Technology

59 Mathematics and Information Sciences

This document was prepared under the sponsorship of the National Aeronautics and Space Administration. Neither the United States Government nor any person acting on behalf of the United States Government assumes any liability resulting from the use of the information contained in this document, or warrants that such use will be free from privately owned rights.

BLANK PAGE

Electronic Components and Circuits

Hardware, Techniques, and Processes

7 Flexible Circuit Boards for Modular Proximity-Sensor Arrays
7 Proximity-Sensor Modules for Use on Flexible Circuit Boards
9 Sferic-Simulating Circuit
9 Readout Schemes To Increase Dynamic Ranges of Image Sensors
11 FET Circuit Monitors Charges Induced by Ionizing Radiation
12 Diffusion-Cooled Hot-Electron Bolometer Mixer
13 Patch Rectenna for Converting Microwave to dc Power
14 Zinc/Air Cell With Collapsible Foam Backing for Anode
14 Photoresponse Diagnosis of Imprint in Ferroelectric Memories
15 Preventing Shrinkage of Gel-Type Zinc Anodes
16 Low-Power, Microprocessor-Controlled Strain-Gauge Circuit
16 Structural Supports for Large Gel-Type Zinc Anodes
17 Improved Separators for Zinc/Air Cells

Flexible Circuit Boards for Modular Proximity-Sensor Arrays

Skinlike coverings of circuit boards and proximity sensors would help robots avoid collisions.

John F. Kennedy Space Center, Florida

Flexible printed-circuit boards and interchangeable electronic proximity-sensor modules that can be plugged into sockets on the boards have been developed to furnish proximity data to collision-avoidance control systems of robots. In typical applications, robot arms would be covered with flexible circuit boards and sensor modules to form skinlike sensor arrays, so that in effect, the arms could "see" nearby objects.

The flexible circuit boards, called "sensorSkin," were designed in coordination with the sensor modules to provide generic sensor circuitry that can readily be configured for different applications. The modules receive digital signals from a control computer and generate digital sensory outputs; this all-digital input/output scheme reduces (in comparison with an analog-signal communication scheme) vulnerability to electronic noise and makes the outputs of a wide variety of sensors compatible with the sensor-data-communication protocol.

Each flexible circuit board can support communication between a control computer and as many as 32 sensor modules, which are described in the following article, "Proximity-Sensor Modules for Use on Flexible Circuit Boards" (KSC-11874). A control computer can be connected to as many as 32 flexible circuit boards via a two-wire communication line, using a hierarchical scheme that enables communication between the computer and a total of as many as 1,023 sensor modules on the 32 circuit boards.

Each flexible circuit board is divided into a rectangular grid of areas called "nodes," each node being allocated to one sensor module (see figure). Each node contains contact holes, into which a socket for a sensor module can be soldered. Redundant power and communication buses are connected to all the nodes. Power is supplied to all the modules on a circuit board via one node. In the hierarchical communication scheme, one module on a circuit board acts as a master, while the others act as slaves. Serial communications between the computer and the slave modules are routed through the master module. Any module can be connected and operated as either the master or one of the slaves. A flexible circuit board can be cut and shaped for a specific application, without loss of function in the remaining nodes. A layer of neoprene rubber and foam insulates the flexible circuit board from the robot arm on which it is mounted.

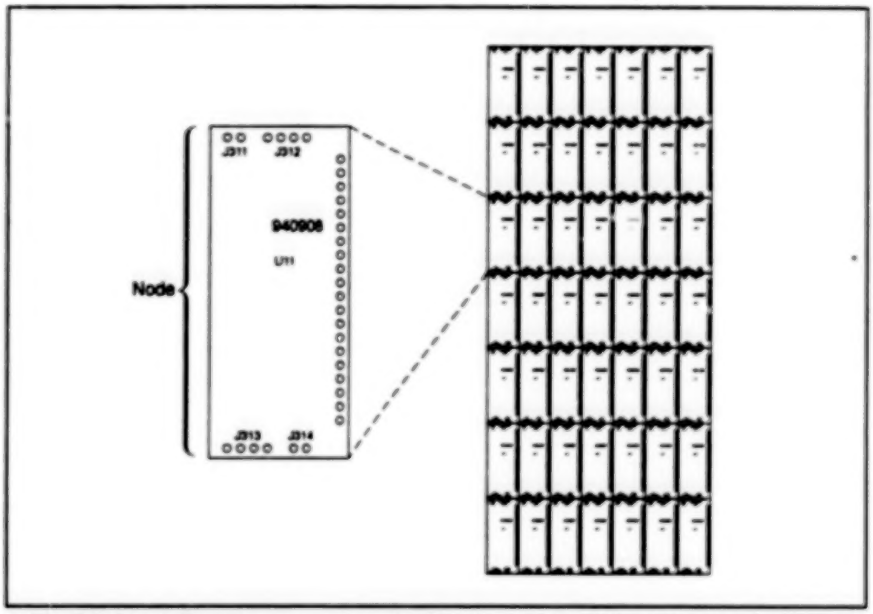

A Flexible Circuit Board measures approximately 12 by 24 in. (30.5 by 61 cm) and contains 49 nodes in a 7 × 7 array. Because of limitations of the applicable serial-data-communication standard, only 32 nodes can be occupied by sensor modules. The extra nodes provide some additional options for positioning sensor modules.

This work was done by Daniel G. Wegerif and Thomas M. Pigoski of Merritt Systems, Inc., for **Kennedy Space Center**. *Further information is contained in a TSP [see page 1].*

In accordance with Public Law 96-517, the contractor has elected to retain title to this invention. Inquiries concerning rights for its commercial use should be addressed to

Tom Pigoski
Merritt Systems, Inc.
435 Gus Hipp Blvd. Bldg B
Rockledge, FL 32955
(407) 632-4968

Refer to KSC-11875, volume and number of this NASA Tech Briefs *issue, and the page number.*

Proximity-Sensor Modules for Use on Flexible Circuit Boards

Modules are interchangeable and compatible with respect to digital communication with a computer.

John F. Kennedy Space Center, Florida

The sensor modules mentioned in the preceding article contain various analog transducer circuits and analog-to-digital converters, plus digital circuits in microcontrollers that communicate with a control computer and relieve the control computer of most of the burden of processing sensor output data. Common microprocessor-based digital circuitry and a shared communications protocol make all of the modules interchangeable and make the specific sensing media invisible to the control computer. These design features are part of a scheme to provide basic sensor systems that can readily be reconfigured and expanded, accelerating and facilitating the development of complex sensor systems for a variety of applications.

Called "smartSensors," the present sensor modules evolved from infrared-sensor modules called "sensorCells," which were described in "Infrared-Proximity-Sensor Modules for Robot" (KSC-11608), *NASA Tech Briefs*, Vol.

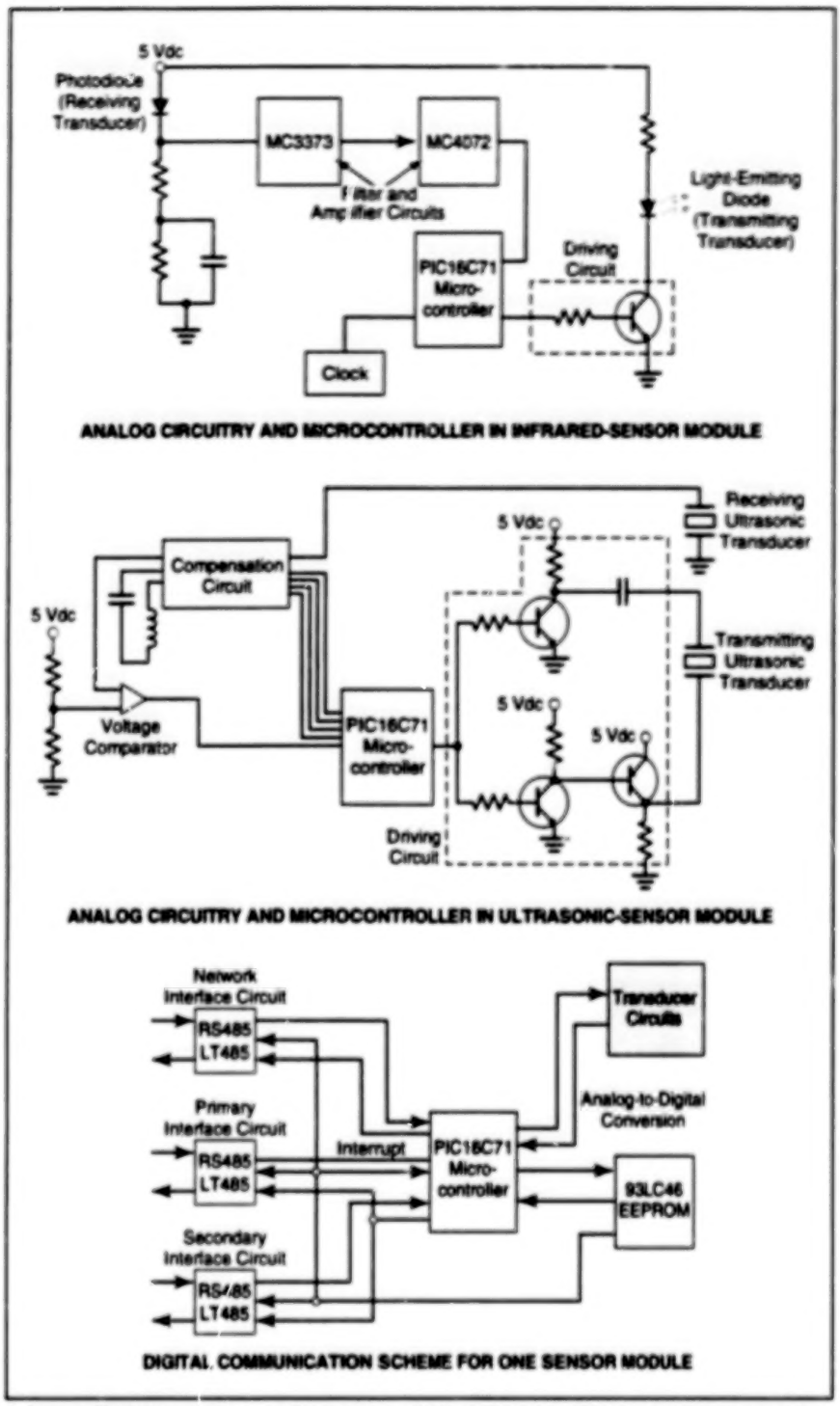

A Sensor Module contains special-purpose analog transducer circuitry, plus general-purpose digital circuitry on a microcontroller that communicates with a control computer through RS-485 serial interface circuits.

19, No. 4 (April 1995), page 13a. Thus far, two prototype modules of the "smartSensor" type have been developed (see figure): One prototype is similar to a module of the "sensorCell" type in that it emits infrared pulses and measures the amplitudes of reflections of the pulses to obtain a crude measure of distance to nearby objects. The other prototype emits ultrasonic pulses and measures the distances of nearby objects from round-trip travel times of reflected pulses.

The analog signal-processing functions specific to the ultrasonic or infrared transmitting and receiving transducers in each module are implemented by special-purpose integrated circuits under the supervision of the microcontroller. Each module also contains a serial electrically erasable, programmable, read-only memory (EEPROM), which stores 16 different calibration tables to enhance performance in different robot configurations or environments. Each calibration table contains (1) fixed information about the type of module (e.g., ultrasonic or infrared), a firmware revision number, and calibration constants; and (2) adjustable parameters regarding transmitted and received signal levels, threshold signal values deemed to be indicative of detection of targets, and the set to which the module belongs. The microcontroller writes data in, and reads data from, the EEPROM on command from the control computer.

The control computer and the microcontrollers in the modules communicate in the hierarchical scheme described in the preceding article, via a common two-wire line according to the RS-485 serial-communication standard. A universal asynchronous receiver/transmitter (UART) is implemented in software in each microcontroller. Communication occurs in a half-duplex mode, in which the communication lines are bidirectional but only one unit — either the control computer or one of the modules — can transmit at a given instant.

Each module operates independently of the others. It waits to receive command information, processes that information, performs the commanded action, and transmits a response if required to do so. The microcontroller has an interrupt capability that gives transmitted or received data total access to the processing resource; this feature makes it possible for the module to communicate at the relatively high rate of 38.6 Kb/s.

This work was done by Daniel G. Wegerif and Thomas M. Pigoski of Merritt Systems, Inc., for **Kennedy Space Center**. *Further information is contained in a TSP [see page 1].*

In accordance with Public Law 96-517, the contractor has elected to retain title to this invention. Inquiries concerning rights for its commercial use should be addressed to

Tom Pigoski
Merritt Systems, Inc.
435 Gus Hipp Blvd. Bldg. B
Rockledge, FL 32955
(407) 632-4968

Refer to KSC-11874, volume and number of this NASA Tech Briefs *issue, and the page number.*

Sferic-Simulating Circuit

This circuit simulates very-low-frequency signals from lightning strikes.

Goddard Space Flight Center, Greenbelt, Maryland

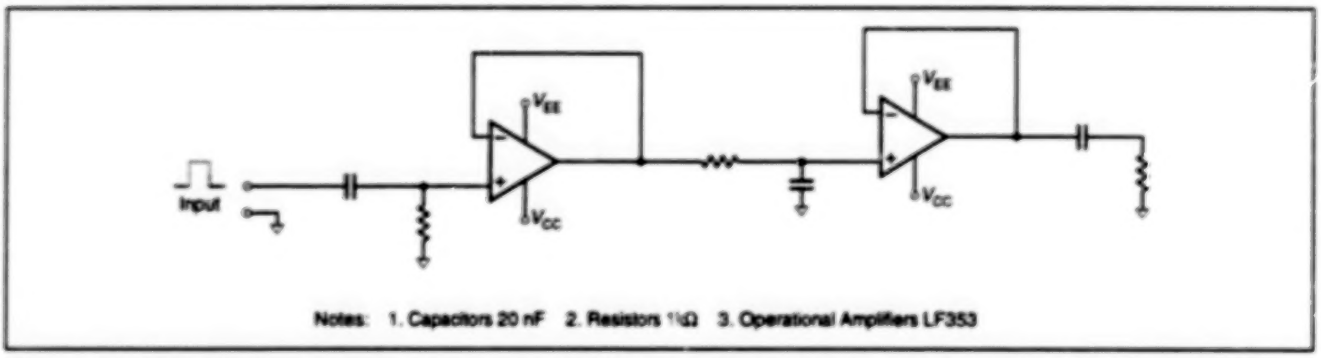

Notes: 1. Capacitors 20 nF 2. Resistors 1 kΩ 3. Operational Amplifiers LF353

Figure 1. The Sferic Simulator generates a bipolar pulse signal like that radiated by lightning when triggered by a fast-rising square wave.

The circuit of Figure 1 generates a signal that simulates the waveform of a sferic — the very-low-frequency electromagnetic signals generated by lightning strikes. This circuit is designed to test and calibrate lightning-detecting instruments.

Typically, lightning-detecting instruments have been calibrated and tested by use of single-frequency signals or broadband noise sources which do not have the spectral characteristics of sferics. This circuit generates a bipolar pulse waveform that closely approximates the main features of sferics (see Figure 2).

The circuit contains few components. The circuit assembly is light in weight and compact; even a "breadboard" version could fit in a square 1.5 in. (about 3.8 cm) on a side.

To insure that the output waveform has the desired shape, the trigger pulse fed to the input terminal of this circuit must be a square wave with rise and fall times less than 100 ns. To prevent coalescence of sequential output pulses, the square-wave pulse-repetition frequency should be kept at or below 3,000 Hz.

This work was done by William M. Farrell and Jeffrey G. Houser of **Goddard Space Flight Center**. *Further information is contained in a TSP [see page 1].*

GSC-13627

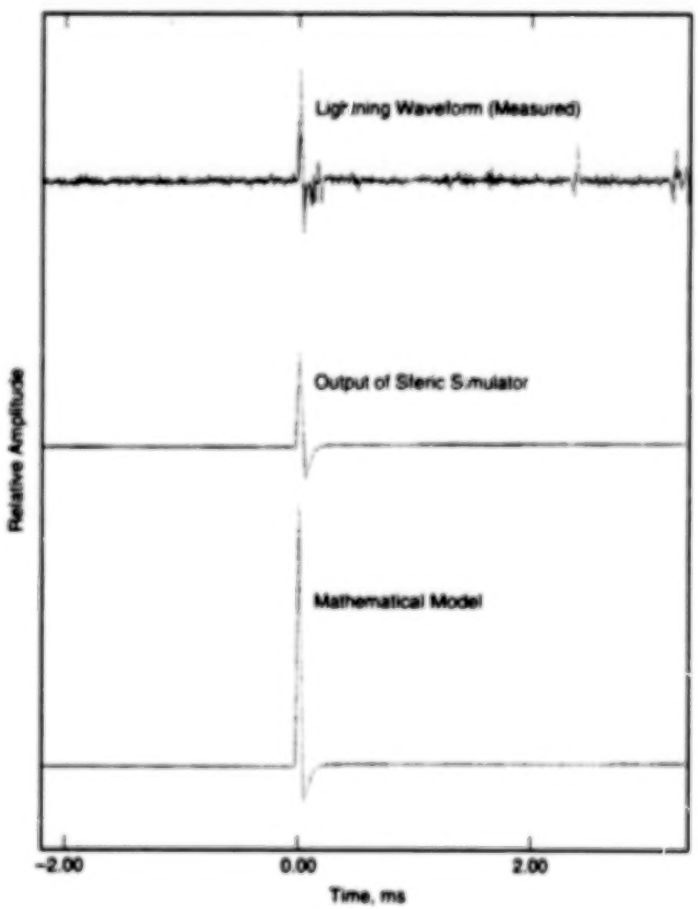

Figure 2. The Output Waveform generated by the sferic simulator resembles a real sferic and a sferic simulated by use of a mathematical model.

Readout Schemes To Increase Dynamic Ranges of Image Sensors

Each pixel would be read out with two or more integration times.

NASA's Jet Propulsion Laboratory, Pasadena, California

Several readout schemes have been proposed to increase the dynamic ranges of active-pixel image sensors. All of these schemes are based on the principle of reading out each pixel with two or more integration times during each frame period.

Active-pixel image sensors are used in advanced video cameras for scientific imaging, and have obvious potential for

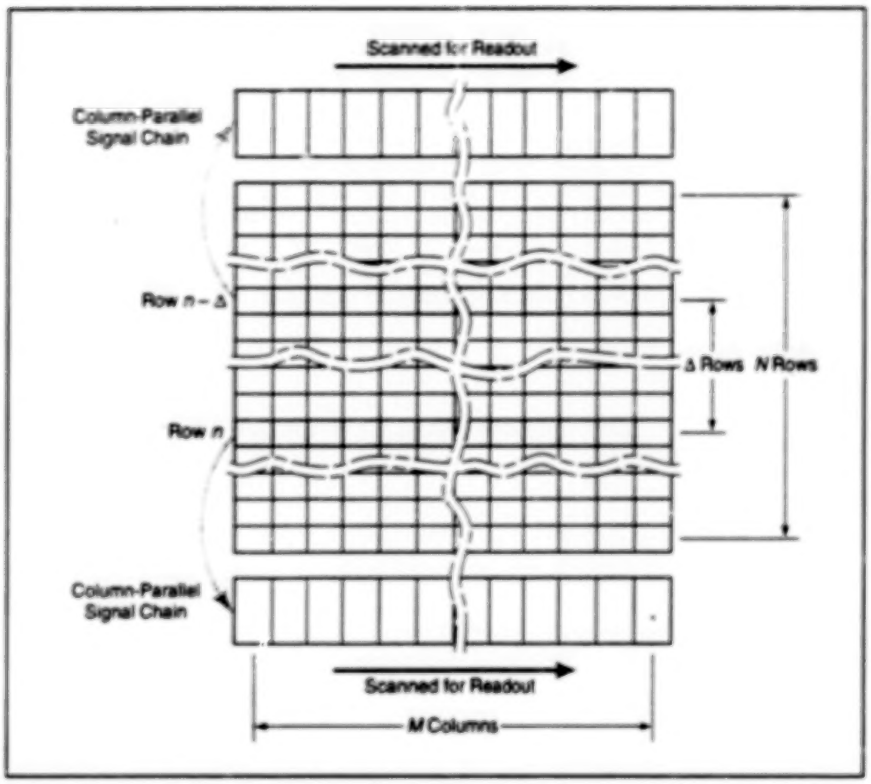

By Simultaneously Reading Out Two Rows of Pixels in the customary sequence, one could obtain two different integration times for each pixel, thereby extending the dynamic range.

numerous applications, including video cameras for digital recording, electronic still and motion photography, and analysis of rapid motions. Shuttering (whether mechanical or electronic) imposes the same exposure (or integration) time on all parts of a scene, and this is inadequate for increasing the dynamic range, as can be understood from a simple example: if the scene includes sunlight and shadows, then shuttering could result in optimum exposure in the sunlit areas with loss of detail in the shadows, or perhaps optimum exposure in the shadows with saturation and thus loss of detail in the sunlit areas.

The proposed method of reading out each pixel with multiple integration times during each frame period raises the possibility that at least one of the integration times might be optimum in the sense that the integrated light-intensity signal would neither be great enough to saturate the photodetector output nor be so small as to be obscured in the noise floor. Thus, a more nearly optimum integration time could be independently selected for each pixel in the image.

Consider an active-pixel image sensor of M columns and N rows. In a conventional readout scheme, the outputs of all M pixels in a row are simultaneously copied onto sampling capacitors at the bottoms of the columns. Thus, each sampling capacitor momentarily contains the readout signal from one pixel. The contents of the sampling capacitors are then transferred out sequentially; this completes the readout from the affected row. Then the next row is selected and the foregoing procedure repeated. After the Nth row has been read out, the frame cycle repeats, starting with readout from the first row. If the total time needed to read out each row is T_{ro}, then the frame period (the time needed to read out all N rows) is simply NT_{ro}. In this conventional scheme, the integration time equals the frame period.

The proposed schemes are best explained by the example of the simplest one (see figure). In this scheme, the rows and columns would be read out in the same sequence as in the conventional scheme, but two rows separated by a vertical distance of Δ pixels would be read out simultaneously. The lower row (denoted the nth row in the figure) would be read out to capacitors at the bottoms of the columns, as in the conventional scheme. The other row [the $(n - \Delta)$th row in the figure] would be similarly read out to capacitors at the tops of the columns.

Because each pixel would be reset at readout to start a new integration process and because the $(n - \Delta)$th row would previously have been read (having previously been the lowermost of the two rows) only Δ row-readout periods ago, the integration time for the $(n - \Delta)$th row would be only ΔT_{ro}. In the case of the nth row, $N - \Delta$ row-readout periods would have elapsed since the previous readout, so that the integration time for the nth row would be $(N - \Delta)T_{ro}$. Thus, there would be two outputs from each pixel: one with integration time $T_1 = (N - \Delta)T_{ro}$, the other with integration time $T_2 = \Delta T_{ro}$. In effect, the dynamic range of each pixel would be extended by the ratio between integration times, $T_1/T_2 = (N - \Delta)/\Delta$.

The other proposed schemes would be extensions and variations of the one described above. For example, instead of reading out two rows simultaneously to two capacitor banks, both rows could be read out alternately to one capacitor bank, at the cost of doubling the frame period. Alternatively, by use of suitably modified column-parallel circuits, the two rows could be read out simultaneously to two capacitor banks, both located at the bottoms of the rows. The concept could be extended to simultaneous or sequential readout from more than two rows to provide a wide selection of integration periods. Still another option might involve resetting each pixel only once per frame period but at other times allowing it to continue integrating and reading it out nondestructively at intervals during the frame period to obtain different integration times. In cases of multiple readouts from the same pixel during the same frame period, it could be desirable to use a buffer memory to make all the data from these readouts come out at the same time.

This work was done by Orly Yadid-Pecht and Eric R. Fossum of Caltech for **NASA's Jet Propulsion Laboratory**. *Further information is contained in a TSP [see page 1].*

In accordance with Public Law 96-517, the contractor has elected to retain title to this invention. Inquiries concerning rights for its commercial use should be addressed to

Larry Gilbert, Director
Technology Transfer
California Institute of Technology
Mail Code 315 - 6
Pasadena, CA 91125
(818) 395-3288

Refer to NPO-19705, volume and number of this NASA Tech Briefs *issue, and the page number.*

FET Circuit Monitors Charges Induced by Ionizing Radiation

This circuit also provides some data on the energy spectrum of ionizing radiation.

NASA's Jet Propulsion Laboratory, Pasadena, California

An integrated circuit that contains field-effect transistors (FETs) provides measurements that indicate the buildup of electric charges, induced by ionizing radiation, in the gate oxides of the FETs. This circuit, called an "integrated charge monitor" (ICM) was designed to be mounted in a geosynchronous communication satellite to obtain data representative of the ionizing-radiation-induced buildup of electric charges in the insulators in FETs in nearby circuits. The data are needed to assess the extent to which radiation-induced charging affects the operation of the nearby FETs. (The buildup of charge can eventually produce arcs, which can cause failure of the associated circuits.) Presumably, a modified version of the ICM could also be used in terrestrial high-radiation environments to assess the effects of ionizing radiation on FET circuits.

The ICM (see figure) contains four p-FETs and two n-FETs. It also includes a radiation-hardened three-bit on-chip multiplexer, which reduces the overall number of external integrated circuits needed to process the ICM readings. A 3.5-kΩ metal resistor is also included on the chip for use in calibrating the multiplexer; this resistor can also be used as a thermometer because its temperature coefficient of resistance is about 14 Ω/°C.

One end of each FET and of the resistor are connected to the terminal labeled "OPI." At any given time, a pair of electronic switches in the multiplexer connects either (a) one of the FETs, (b) the metal resistor, or (c) the terminal labeled "EXT" to the terminals labeled "OPO" and "VSEN." The multiplexer switch selection is controlled by external digital signals via terminals A0, A1, and A2. External circuitry supplies a constant current via terminals OPI and OPO to excite the selected FET or resistor, and the voltage across the selected device is fed to external circuitry through terminal VSEN. This current (100 μA) and the offset voltage (1.5 V) are chosen so that the p-FETs operate at their temperature-independent points.

The charges that build up in the oxide and at the oxide/silicon interface of each FET cause a shift in the threshold voltage and an increase in the density of interface states. The n-FETs are used to evaluate the onset of radiation-induced failures. Each p-FET is covered with a Kovar (or equivalent) radiation shield, which serves two purposes: First, each shield prolongs the operating life of its FET in the high-radiation environment. Second, the four shields are of different thicknesses, and the thicker a shield, the more it discriminates against lower-energy ionizing particles. Thus, the readings from the four differently shielded p-FETs also contain some information on the energy spectrum of the ionizing radiation.

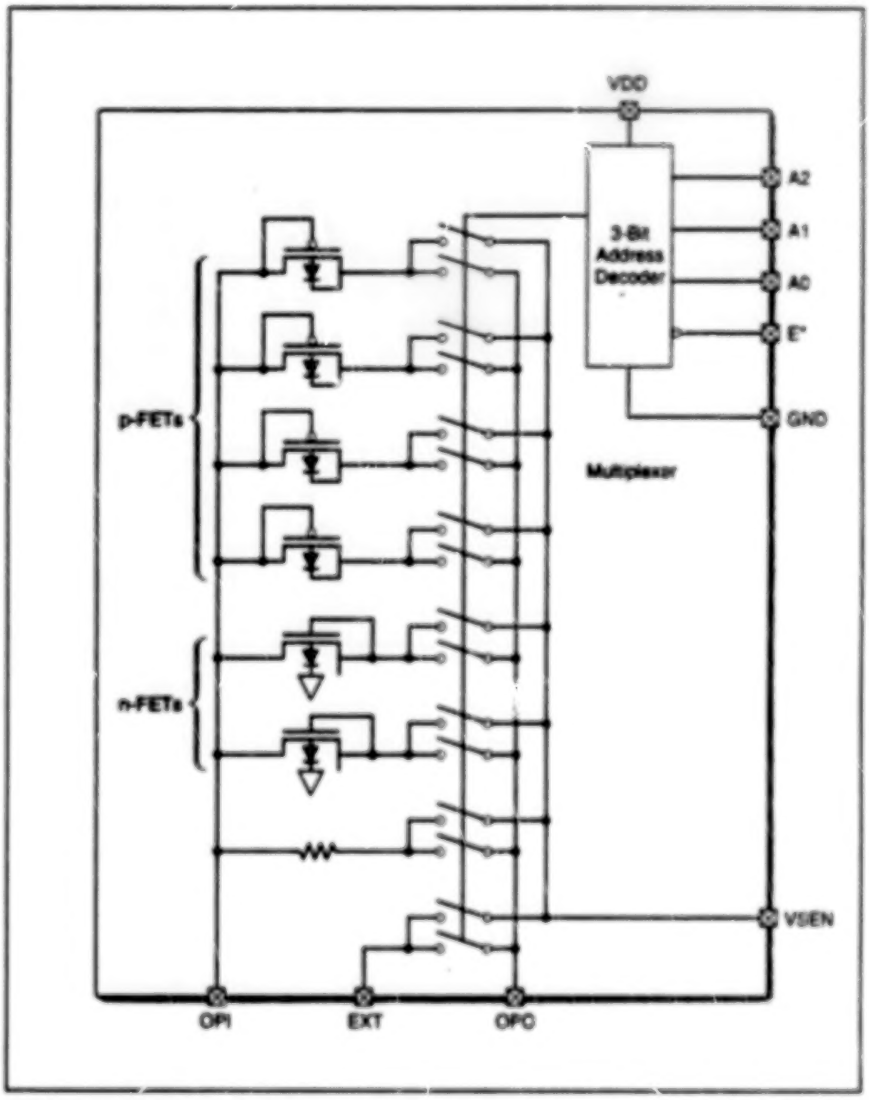

The Integrated Charge Monitor contains FETs that are used to sample the effects of ionizing-radiation-induced charging of insulators in other, nearby FETs.

This work was done by Martin G. Buehler, Brent R. Blaes, and George A. Soli of Caltech for **NASA's Jet Propulsion Laboratory**. *Further information is contained in a TSP [see page 1].*

In accordance with Public Law 96-517, the contractor has elected to retain title to this invention. Inquiries concerning rights for its commercial use should be addressed to

Larry Gilbert, Director
Technology Transfer
California Institute of Technology
Mail Code 315 - 6
Pasadena, CA 91125
(818) 395-3288

Refer to NPO-19482, volume and number of this NASA Tech Briefs issue, and the page number.

Diffusion-Cooled Hot-Electron Bolometer Mixer

The mixer output frequency can range up to a few gigahertz.

NASA's Jet Propulsion Laboratory, Pasadena, California

A superconducting hot-electron bolometer has been constructed as a prototype of frequency-mixing devices that could operate at carrier and local-oscillator frequencies exceeding 1 THz, putting out signals at intermediate frequencies (IFs) up to a few gigahertz. The most likely initial applications of such mixers would occur in radio-astronomy receivers, wherein IF bandwidths of at least 1 GHz are needed for molecular-line spectroscopy.

The mixing process in a superconducting hot-electron bolometer relies on heating of the electron gas. Consequently, unlike a superconductor/insulator/superconductor (SIS) tunnel-junction mixer, the bolometer mixer does not have an upper frequency limit related to the superconductive energy gap (indeed it absorbs power more nearly uniformly at frequencies above the gap frequency). Until recently, hot-electron bolometers have not been extensively used as heterodyne mixers because of a limitation imposed on the IF bandwidth by the thermal-relaxation time of heated electrons in bulk devices. In bulk indium antimonide bolometers, for example, the IF rolloff frequency is only about 1 MHz. Recently, hot-electron bolometers containing very thin superconductive films have been proposed to achieve practical IF bandwidths of several GHz. Bolometer mixers containing thin NbN films and relying on electron/phonon interactions to cool the electrons have recently exhibited IF bandwidths near 700 MHz.

The present device (see Figure 1) differs from older superconducting hot-electron bolometers in that the thermal conductance that cools the heated electrons is provided by rapid electron diffusion rather than phonon emission. To achieve the short electron diffusion time required for a high IF bandwidth, the superconducting circuit element (in this case, a strip of niobium) is made very short (about 0.28 μm), with a width of about 0.14 μm. The Nb film is also made very thin (10 nm) to place it in the "dirty" limit, in which the very short mean free path (1 to 10 nm) enhances electron/electron interactions relative to electron/phonon interactions. Thus, when absorbing RF power, the electron gas can thermalize at a temperature higher than that of the Nb lattice. The small electron specific heat and the high thermal conductance provided by diffusion result in a very short thermal response time — about 55 ps — and a corresponding 3-dB IF rolloff frequency between 2 and 3 GHz.

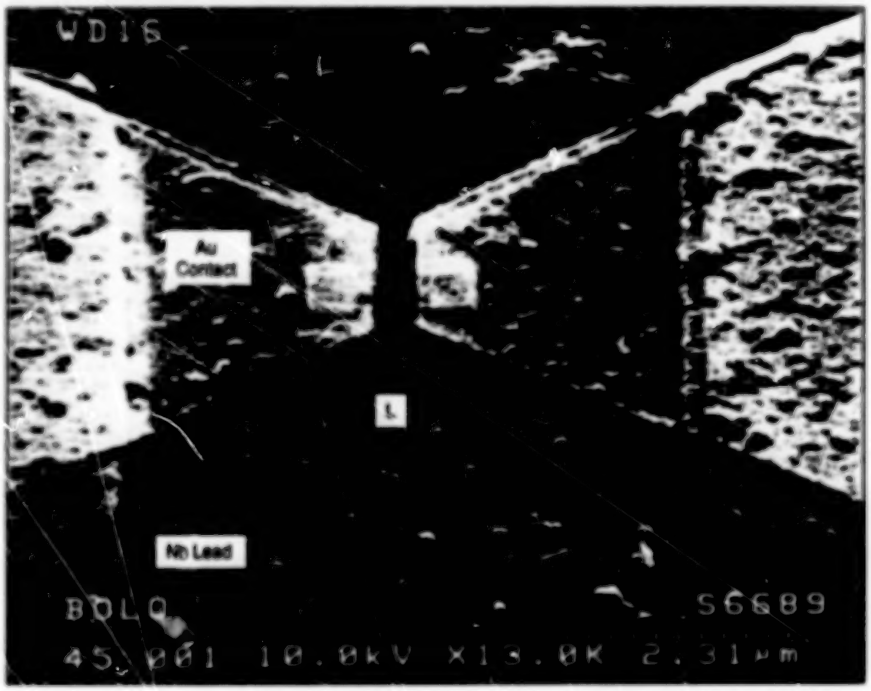

Figure 1. The Thin Strip of Niobium is the heart of the diffusion-cooled hot-electron bolometer.

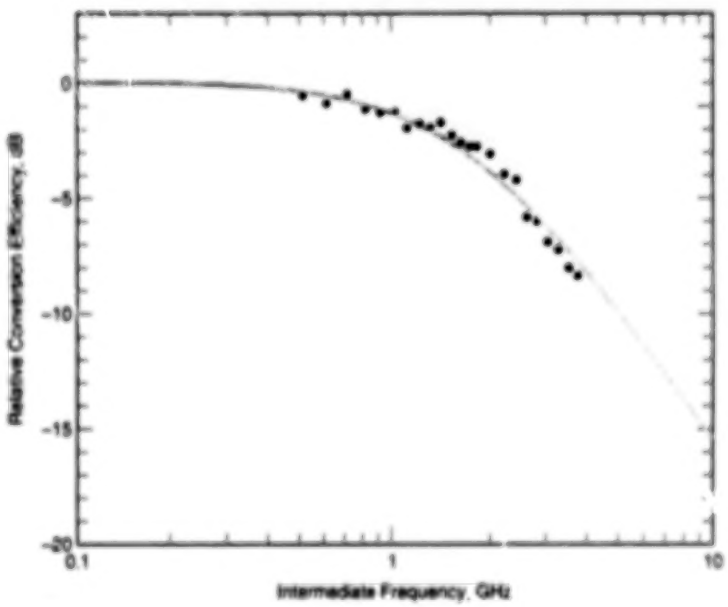

Figure 2. The Curve Fitted to the Data Points is characterized by a 3-dB rolloff frequency of 1.7 GHz.

To prevent Andreev reflections, which could increase the response time of the device, both ends of the Nb are placed in contact with normal conductive metal films (Au films 100 nm thick) rather than superconductors. The gold films, in turn, are in contact with a waveguide probe and a filter circuit patterned from a 110-nm-thick Nb layer. The device was fabricated on a fused-quartz substrate. The superconducting transition of the Nb film is centered at a critical temperature (T_c) of ~4.7 K, with a transition width of ~1.2 K (in a thin dirty

film of Nb, the T_C is suppressed relative to the bulk T_C value of about 9.2 K).

In preparation for tests, the device was mounted in a waveguide mixer block that was cooled to a temperature of 2.2 K. Using a multiplier chain driven by a Gunn oscillator to generate local oscillator power at 533 GHz, and hot and cold black-body radiators as calibrated weak signal sources, the output intermediate frequency response was measured. The measurements yielded a lowest receiver noise temperature of 650 K and an estimated conversion efficiency of −11.4 dB (double sideband) at a local-oscillator frequency of 533 GHz. The 3-dB rolloff in conversion efficiency in the IF band was found to lie between 1.7 and 1.9 GHz (see Figure 2), depending slightly on the dc bias point of the bolometer. The upper limit of the superconducting-transition temperature range (5.3 K) corresponds to a superconducting gap frequency of 410 GHz, which is well below that of the mixing experiments.

This work was done by Anders Skalare, William McGrath, Bruce Bumble, and Henry LeDuc of Caltech and Peter Burke, A. A. Verheijen, and Daniel Prober of Yale University for **NASA's Jet Propulsion Laboratory**. *Further information is contained in a TSP [see page 1].*

NPO-19719

Patch Rectenna for Converting Microwave to dc Power

The antenna and microstrip filter and rectifier circuitry are mounted on dielectric substrates.

NASA's Jet Propulsion Laboratory, Pasadena, California

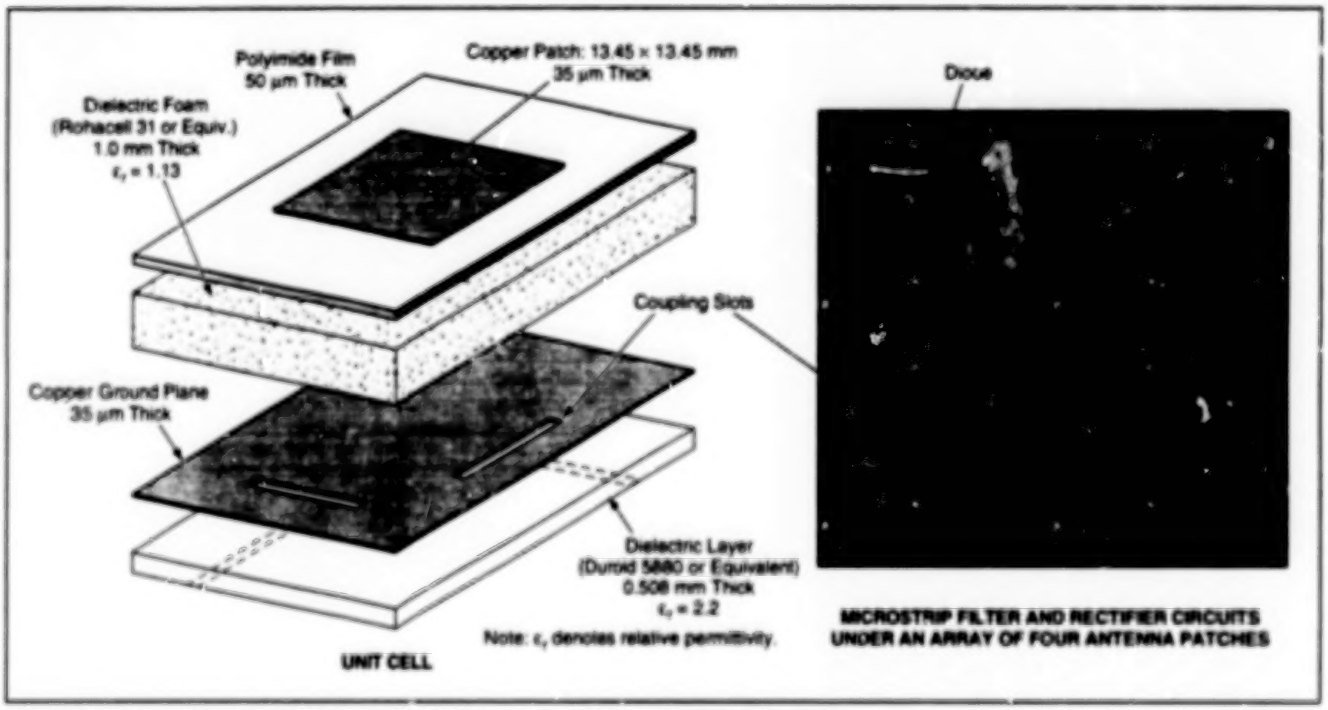

Multiple Square Units are joined in a planar array to receive and rectify microwave power.

A lightweight planar structure contains an antenna for receiving microwave power, plus filter and rectifier circuitry for converting the microwave power to dc. This antenna is a prototype component of systems for wireless delivery of electric power in industrial applications and perhaps to airborne instrumentation.

The antenna structure (see figure) comprises a square planar array of identical unit cells. The antenna is configured to receive microwave power in two orthogonal linear polarizations and is thus also able to receive in circular polarization. The basic antenna elements are square copper patches, which are above and separated from a copper ground plane by a layer of dielectric material. The filter and rectifier circuits and the dc output coupling conductors are registered with the overlying antenna patches and are located below the ground plane, separated from the ground plane by another layer of dielectric material.

Coupling between each antenna patch and its underlying filter and rectifier circuit takes place via two orthogonal slots in the ground plane; this coupling scheme eliminates the need for via holes and conductors, thus facilitating construction with simple sheets of lightweight dielectric foam. The filter and rectifier circuits are implemented as a square array of microstrip impedance-matching transmission lines, butterfly-shaped microstrip filters, and rectifying diodes. The nearby ground plane improves the thermal performance of the circuitry. The overall resonant response of the square antenna patches and the filter circuits helps to suppress both harmonic radiation and coupling to unwanted source frequencies. Tests under various conditions at a frequency of 8.51 GHz indicated overall power-conversion efficiencies ranging from about 25 to about 61 percent.

This work was done by Larry W. Epp, Hugh K. Smith, Abdur R. Khan, and R. Peter Smith of Caltech for **NASA's Jet Propulsion Laboratory**. *Further information is contained in a TSP [see page 1].*

In accordance with Public Law 96-517, the contractor has elected to retain title to this invention. Inquiries concerning rights for its commercial use should be addressed to

Larry Gilbert, Director
Technology Transfer
California Institute of Technology
Mail Code 315-6
Pasadena, CA 91125
(818) 395-3288

Refer to NPO-19580, volume and number of this NASA Tech Briefs issue, and the page number.

Zinc/Air Cell With Collapsible Foam Backing for Anode

The foam backing yields to accommodate expansion of the anode during discharge.

Lyndon B. Johnson Space Center, Houston, Texas

The figure shows an example of a zinc/air electrochemical power cell that incorporates a collapsible foam backing for the anode. The anode (as zinc powder) is an integral part of a gel-material unitary electrode component that also contains the electrolyte (an aqueous solution of potassium hydroxide) and a gelling agent. During discharge, the zinc is oxidized, and the resulting zinc oxide occupies more volume than the zinc does. The volume of the anode at full discharge is about 20 percent greater than when the cell was fresh.

If expansion space is not provided in the cell, this expansion of the anode during discharge can cause bulging and even rupturing of the cell, and rupturing can cause leakage of electrolyte. The foam backing provides some structural support for the anode, and yields to accommodate the expansion of the anode.

The foam is supported by a plastic tray with small holes. A porous hydrophobic membrane is placed under the foam to cover the holes, and the edges of the membrane are sealed to the tray. Gases squeezed out of the foam by expansion of the anode are vented through the holes. The membrane allows the gases, but not the electrolyte, to flow through the holes.

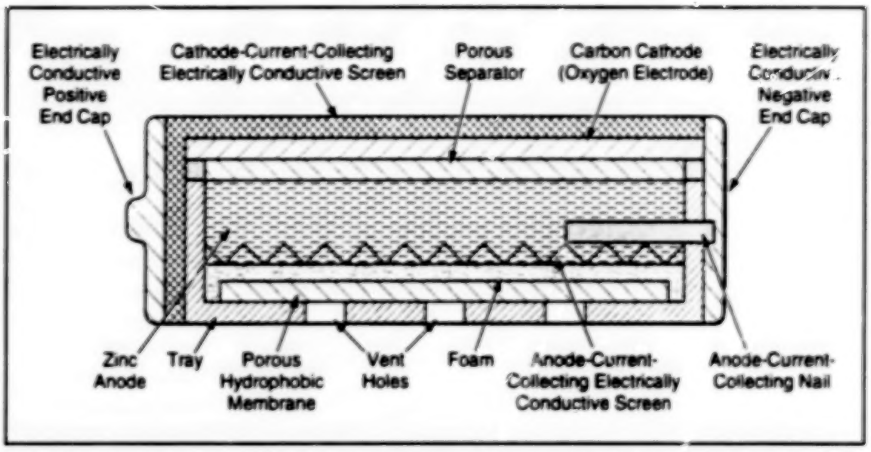

The Foam Yields To Accommodate Expansion of the Anode during discharge of the cell. **The hydrophobic membrane allows gases to be vented through the holes but prevents leakage of electrolyte.**

This work was done by Ronald A. Putt of Matsi, Inc., for **Johnson Space Center**. *Further information is contained in a TSP [see page 1].*

In accordance with Public Law 96-517, the contractor has elected to retain title to this invention. Inquiries concerning rights for its commercial use should be addressed to

Matsi, Inc.
Glenn Woodruff, President
430 10th St. NW, Suite S-007
Atlanta, GA 30318-5768
(404) 876-8009

Refer to MSC-22437, volume and number of this NASA Tech Briefs *issue, and the page number.*

Photoresponse Diagnosis of Imprint in Ferroelectric Memories

Another use for nondestructive optical readout has been proposed.

NASA's Jet Propulsion Laboratory, Pasadena, California

Nondestructive optoelectronic probing could be harnessed as a powerful tool to study the basic physical mechanisms of a phenomenon called "imprint" that has been observed in developmental ferroelectric thin-film memory devices. Aspects of these devices and of the nondestructive optoelectronic probing and readout of these devices have been described in several previous articles in *NASA Tech Briefs*, including "Noninvasive Optical Probe of Ferroelectric Films" (NPO-18549), Vol. 17, No. 5, page 54; "Improved Ferroelectric Memories With Nondestructive Readout" (NPO-19033), Vol. 18, No. 11, page 40; "Photonic Diagnostic Technique for Thin Photoactive Films" (NPO-19393), Vol. 20, No. 4, page 49; "Ultra-High-Density Ferroelectric Memories" (NPO-19265), Vol. 19, No. 9, page 60; and "Multilayer Thin-Film Microcapacitors" (NPO-19403), Vol. 19, No. 9, page 19a.

An element of a memory device of the type considered here is a thin-film ferroelectric capacitor, in which nonvolatile storage of a datum (an analog value or a digital bit) is effected by use of remanent polarization in a designated region in a ferroelectric film. When one attempts to erase a bit that has been stored for a long time, one may not succeed; that is, sometimes, the polarization cannot be reversed: this is what is meant by "imprint" in the present context. Obviously, imprint may present a formidable obstacle to the development of ferroelectric nonvolatile memory devices.

It has been conjectured that imprint is caused by the irreversible, gradual, cumulative migration of defects (e.g., oxygen vacancies) and/or electrically charged species under the combined influences of electric field and temperature. Imprint is suspected to arise due to existence of *a*-axis inclusions (90° domain walls) in an otherwise *c*-axis oriented structure, as required for good memory performance. The photoresponse is sensitivity dependent on the orientation and therefore any presence of *a*-axis inclusions can be diagnosed by occurrence of a larger response.

The nondestructive optoelectronic probing technique (see figure) is particularly suited for tracking the evolution of the internal fields within a thin ferroelectric film as a function of operational history, storage time, and environmental history. In so doing, it also serves as a unique probe for studying the physical mechanisms that cause imprint. The nondestructive optical probing technique may also constitute the basis of a testing instrument for use in

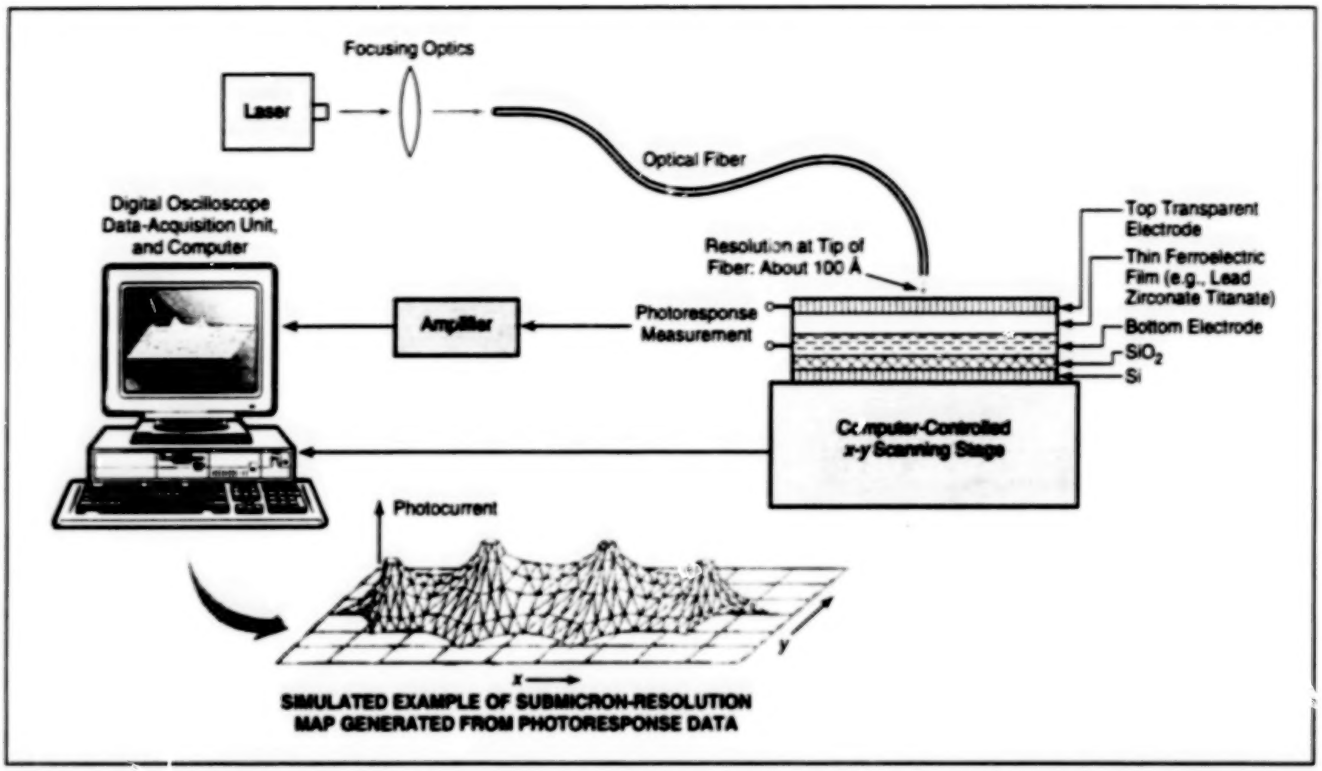

The **Thin Ferroelectric Film Under Test** is sandwiched between two electrodes, as in a capacitor, and the desired spot in the film is positioned under an optical-fiber probe that delivers pulsed laser light concentrated into the spot. Typically, the pulses are about 10 ns long. To prevent perturbation of electric polarization in the film, the laser wavelength is chosen so that the photon energy is less than the bandgap of the ferroelectric material.

manufacturing ferroelectric nonvolatile memory devices: Such an instrument could be used to screen the devices for imprint without fatiguing the devices.

This work was done by Sarita Thakoor of Caltech for **NASA's Jet Propulsion Laboratory**. *Further information is contained in a TSP [see page 1].*

In accordance with Public Law 96-517, the contractor has elected to retain title to this invention. Inquiries concerning rights for its commercial use should be addressed to

Larry Gilbert, Director
Technology Transfer
California Institute of Technology
Mail Code 315 - 6
Pasadena, CA 91125
(818) 395-3288

Refer to NPO-19212, volume and number of this NASA Tech Briefs *issue, and the page number.*

Preventing Shrinkage of Gel-Type Zinc Anodes

A chemically inert filler is used.

Lyndon B. Johnson Space Center, Houston, Texas

Tests show that a chemically inert filler in gel-type zinc anodes in electrochemical power cells helps to preserve the discharge capacity that would otherwise be lost as a result of dryout during long storage. This is an important development because gel-type zinc anodes are used in the popular commercial alkaline/manganese dioxide power cells.

In making a gel-type zinc anode, zinc powder is blended with a potassium hydroxide electrolyte that contains a gelling agent. Some cells that contain gel-type zinc anodes lose more than 50 percent of original discharge capacity in this way. The loss of capacity has been attributed to shrinkage of the gelled anodes away from separators and cathodes; the air gaps caused by the shrinkage prevent the anodes from discharging efficiently at design current densities.

One suitable chemically inert filler material is Grade 31 White Nylon Flock (or equivalent). When added to an anode in a suitable amount (2 weight percent), this material causes the anode volume to remain the same, wet or dry, yet does not physically bind the electrolyte or the solvent water and does not degrade electrochemical performance.

This work was done by Ronald A. Putt of Matsi, Inc., for **Johnson Space Center**. *Further information is contained in a TSP [see page 1].*

In accordance with Public Law 96-517, the contractor has elected to retain title to this invention. Inquiries concerning rights for its commercial use should be addressed to

Matsi, Inc.
Glenn Woodruff, President
430 10th St. NW, Suite S-007
Atlanta, GA 30318-5768
(404) 876-8009

Refer to MSC-22439, volume and number of this NASA Tech Briefs *issue, and the page number.*

Low-Power, Microprocessor-Controlled Strain-Gauge Circuit

Power is turned on briefly during sampling periods.

NASA's Jet Propulsion Laboratory, Pasadena, California

A microprocessor-controlled strain-gauge circuit operates intermittently to save energy. The circuit is designed to be energized by a 9-V battery of the type commonly used in many commercial electronic circuits.

Because a typical strain gauge has a resistance of about 120 Ω, it draws a current of about 75 mA from a 9-V battery. At this level of current, if the gauge operates continuously, it quickly discharges the battery. A typical strain-gauge circuit also includes an amplifier, which contributes further to the drain on the battery. By operating intermittently at full power instead of continuously, the present circuit consumes less time-averaged power.

This circuit includes a strain gauge in a Wheatstone bridge, an electronic switch, an amplifier, a multiplexer, and a microprocessor. The microprocessor includes timing circuitry that controls the intermittent operation of the rest of the microprocessor, the amplifier, the multiplexer, and the Wheatstone bridge. Under control of the timing circuitry, the electronic switch applies battery voltage to the Wheatstone bridge only during brief sampling periods. The amplifier and the part of the microprocessor that processes the gauge readings are also turned on only during the sampling periods.

During each sampling period, the timing-and-control part of the microprocessor coordinates the operation of the multiplexer and the rest of the microprocessor to make the rest of the microprocessor read (1) the voltage applied to the Wheatstone bridge, then (2) the amplified output from the bridge. The microprocessor then divides the amplified output of the bridge by the voltage applied to the bridge to obtain a normalized strain reading that is independent of any decrease in battery voltage and of any voltage drop in the electronic switch.

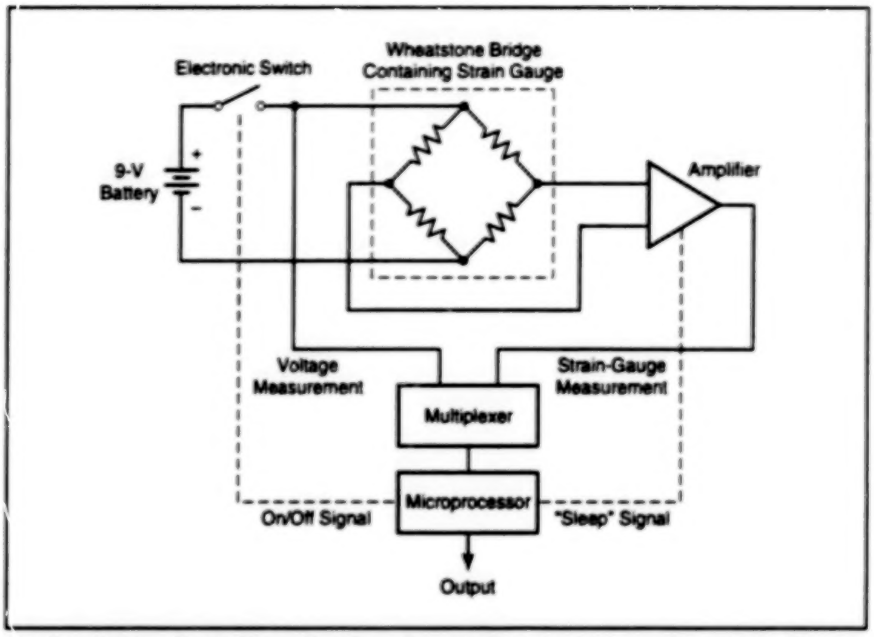

This Circuit Takes Strain-Gauge Readings Repeatedly during brief sampling periods. The rest of the time, the main power-consuming parts of the circuit are turned off. Thus, the time-averaged power consumption is much less than that of a continuously operating strain-gauge circuit.

The sampling rate can be set at any value up to several hundred hertz; for example, a prototype of the circuit operated at a sampling rate of 300 Hz and was found to be capable of yielding data on vibrations at frequencies up to 30 Hz. The decrease in power consumption depends on the sampling rate and the duration of the sampling period. The power consumed by this circuit in typical applications could range from about 1/100 to as little as 1/1,000 the power consumed by a continuously operating strain-gauge circuit.

This work was done by Harold Kirkham and Shannon Jackson of Caltech for **NASA's Jet Propulsion Laboratory**. *Further information is contained in a TSP [see page 1].*
NPO-19750

Structural Supports for Large Gel-Type Zinc Anodes

These supports hold anodes firmly against separators and cathodes.

Lyndon B. Johnson Space Center, Houston, Texas

Structural members have been devised to provide additional support for gel-type zinc anodes in large electrochemical power cells like the larger versions of the popular commercial button- and prism-shaped zinc/air cells. Previously, cells of this type with diameters greater than about 0.5 in. (1.3 cm) had been observed to lose more than about half their initial discharge capacities when exposed to the shocks and vibrations of normal handling and transport.

These losses of discharge capacity were attributed to the formation of gaps between the anodes and the adjacent separator-and-cathode structures. The gaps made it impossible to take full advantage of the large surface areas and ample interstitial electrolyte offered by gelled zinc anodes. The gaps, in turn, were attributed to two causes:

1. Although the gel-type zinc anodes are highly viscous, they are nevertheless fluid and capable of movement.
2. A volume filled with a mat or a foam pad had been provided on the back of each anode (on the side of the anode opposite the separator) to accommodate expansion of the anode during discharge. During handling and transport, the anode tended to move into this space; the pad or mat did not provide firm enough support to prevent such movement.

The present concept of adding structural members to provide additional

support to anodes was influenced by the observation that in smaller cells, the viscosity of the anode material appears to suffice to hold the anodes in place. Accordingly, such a structural member typically consists of a honeycomb or a serpentine ribbon that divides the anode gel into relatively small pockets that are held firmly in place against the separator. The member rests directly on the bottom of the cell and rises to meet the separator and the cathode. If the member is made of copper, zinc, or brass, it can also serve as the anode current collector, thereby improving the collection of current and eliminating the need for additional current-collecting parts.

This work was done by Ronald A. Putt of Matsi, Inc., for **Johnson Space Center**. *Further information is contained in a TSP [see page 1].*

In accordance with Public Law 96-517, the contractor has elected to retain title to this invention. Inquiries concerning rights for its commercial use should be addressed to

Matsi, Inc.
Glenn Woodruff, President
430 10th St. NW, Suite S-007
Atlanta, GA 30318-5768
(404) 876-8009

Refer to MSC-22438, volume and number of this NASA Tech Briefs *issue, and the page number.*

Improved Separators for Zinc/Air Cells

Anode utilization is increased significantly.

Lyndon B. Johnson Space Center, Houston, Texas

Improved separators have been conceived for use between the zinc and oxygen electrodes in zinc/air electrochemical power cells. The improved separators reduce oxidation of the zinc electrodes, thereby helping to preserve anode utilization and discharge capacity.

The separators in common use (e.g., Celgard®) are microporous and are used to prevent electrical short circuits between the zinc and oxygen electrodes. While the microporous separators prevent shorting, they allow oxygen gas to reach and chemically attack the zinc during operation. The resulting oxidation of the zinc can reduce cell capacity by as much as 50 percent. The rate of attack by oxygen in a fresh cell is relatively low, but increases during discharge as the zinc electrode becomes drier and the zinc oxide discharge product exposes increasing surface area to attack.

According to the present concept of improved separators, the microporous separator in a cell is either replaced by, or augmented with, a semi-permeable membrane that allows passage of ions and other dissolved species, but not of gaseous oxygen. Examples of such semipermeable membranes include ion-exchange membranes and cellophane. In a test of this concept, a cellophane membrane was added to a microporous separator in a prismatic zinc/air cell. As a result of this modification, the anode utilization was increased, from the previous range of 50 to 80 percent, to a value over 90 percent.

This work was done by Ronald A. Putt of Matsi, Inc., for **Johnson Space Center**. *No further documentation is available.*

In accordance with Public Law 96-517, the contractor has elected to retain title to this invention. Inquiries concerning rights for its commercial use should be addressed to

Matsi, Inc.
Glenn Woodruff, President
430 10th St. NW, Suite S-007
Atlanta, GA 30318-5768
(404) 876-8009

Refer to MSC-22440, volume and number of this NASA Tech Briefs *issue, and the page number.*

BLANK PAGE

Electronic Systems

Hardware, Techniques, and Processes

21 Null-Stabilized Active Hand Controller
21 Dual-Photodiode Edge-Displacement Sensor
22 Microwave Measurements of Speeds of Food Particles in Pipes
23 Automated Testing of Solar Photovoltaic Arrays
24 Fiber-Optic Data Bus for a Sensor Network

BLANK PAGE

Null-Stabilized Active Hand Controller

Oscillations are suppressed without loss of crisp feel.

Lyndon B. Johnson Space Center, Houston, Texas

An improved active hand controller retains stability in its null zone without loss of crisp feel in the operator's hand. The control principle may be suitable for a variety of hand-controlled vehicles, including motorized wheelchairs.

In general, an active hand controller tends to become unstable in its null zone, where its force-versus-displacement curve passes through zero, because of nonlinearity in the curve and backlash in an associated gear train. The usual remedy is to employ rate damping, which desirably enhances stability but undesirably slows transient response. In addition, excessive rate damping makes a hand controller feel viscous or sluggish to the user.

In the improved active hand controller, rate damping is increased only in a small region about null. A breakout circuit (see figure) produces a discrete breakout torque command, either positive or negative, depending on whether the position signal is positive or negative. Unless the position signal is exactly zero, the breakout amplifier commands a large motor torque. A comparator controls a switch that increases or decreases the gain of the rate-control loop, depending on the position of the control actuator. When the position is within a small region around null, the comparator increases the rate-control-loop gain, damping out the oscillations that occur at null.

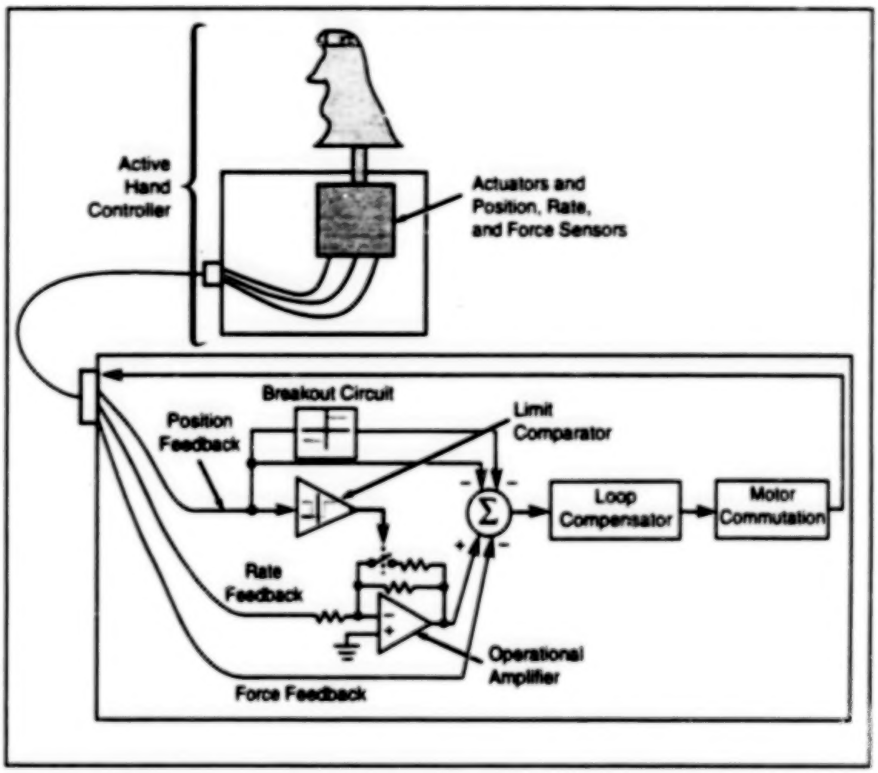

The Control Circuitry associated with the improved active hand controller includes a limit comparator that commands an increase in rate damping near the null position.

This work was done by William W. Gregory and James Kauffman of Honeywell, Inc., for **Johnson Space Center**. *Further information is contained in a TSP [see page 1].*

MSC-22131

Dual-Photodiode Edge-Displacement Sensor

Precision is enhanced by subtraction to cancel correlated noise components.

Marshall Space Flight Center, Alabama

The figure schematically illustrates an optoelectronic sensor that measures the lateral displacement of an edge; e.g., the deflection at the tip of a cantilever beam. Light (preferably coherent) from a laser diode or other source is carried to the edge by a fiber-optic cable. The light emerges from the tip of the fiber-optic cable, illuminating a nearby dual photodiode. The dual photodiode faces the edge, positioned with the centerline between the two photodiode segments facing approximately the nominal zero-displacement position of the edge. The fraction of the available luminous flux incident on each photodiode segment depends on the displacement of the edge relative to the centerline. Thus, the displacement can be determined from the difference between the output currents of the photodiodes.

The output currents of the photodiodes are converted to voltage drops across resistors, and these voltage drops are fed to the two input terminals of a differential amplifier. The output of the differential amplifier is digitized and sent to a computer.

The dual photodiode features a common-cathode design; that is, one photocathode serves as the source of electrons for both segments of the photodiode. Because of their common origin, the electronic noise (shot noise) currents in both photodiode segments are correlated with each other to a significant degree. This is an advantage because the subtraction of signals in the differential amplifier causes mutual cancellation of the correlated noise components, thereby reducing the noise in the amplified output signal, relative to the noise that would remain if two separate photodiodes (with uncorrelated noise currents) were used. As a result, the precision of the displacement measurement is enhanced.

The use of a coherent source of light in conjunction with the common-photocathode dual photodiode also helps to minimize the net output noise: Any fluctuations in the output of such a source result in correlated fluctuations in the illumination of the segments of the photodiode. The resulting correlated fluctuating components of the output signal are canceled in

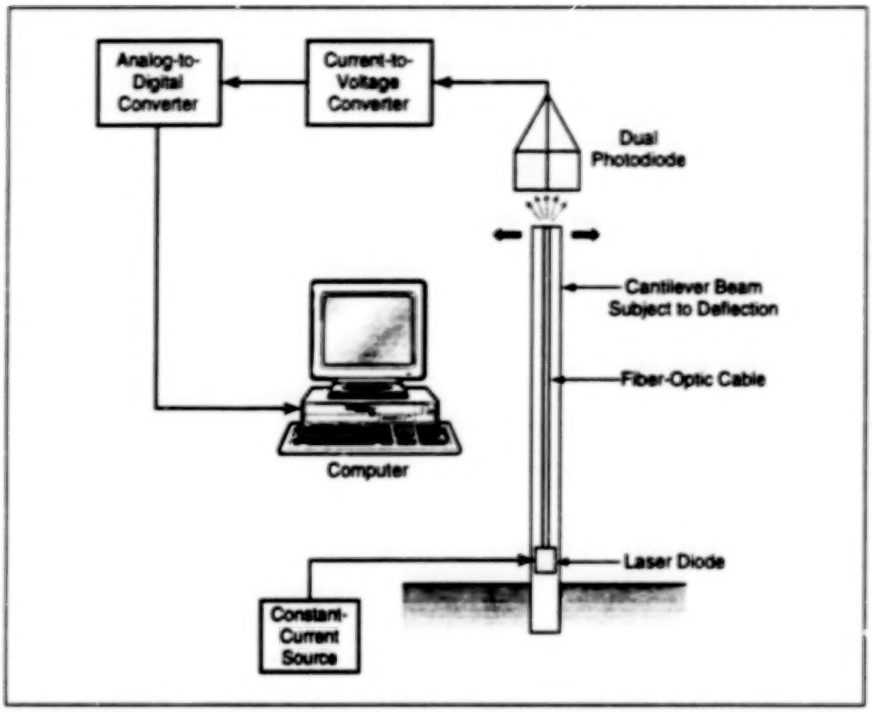

This Edge-Displacement Sensor achieves low-noise output by use of a coherent light source, a dual photodiode with a common photocathode, and differential amplification to suppress correlated noise components.

the same manner as that of the correlated shot-noise components.

The computer processes the digitized output of the differential amplifier into an indication of displacement. This processing involves mainly lookup and interpolation in a set of displacement-vs.-differential-output calibration data. Calibration is accomplished with the help of a translation stage that can be used to displace the edge to known positions. The first step in calibration is to establish the zero-displacement (preferably the zero-differential-output) position. Then the edge is displaced to other known positions, where the differential output values are recorded for use as calibration data.

This work was done by John L. Remo of Quantametrics for **Marshall Space Flight Center**. *Further information is contained in a TSP [see page 1].*

Inquiries concerning rights for the commercial use of this invention should be addressed to the Patent Counsel, Marshall Space Flight Center [see page 1]. Refer to MFS-26412.

Microwave Measurements of Speeds of Food Particles in Pipes

These measurements would help to ensure sterilization in food-processing plants.

Lyndon B. Johnson Space Center, Houston, Texas

Microwaves can be used to measure the times of transit of selected food particles along pipes in industrial food-processing equipment. Typically, a food mixture pumped along such a pipe consists of liquid and solid components at a temperature of 270 to 285 °F (132 to 141 °C) and pressure of 60 psig (gauge pressure of 0.41 MPa). The purpose of measuring transit times is to determine whether the food has been kept hot enough for a time long enough to ensure sterilization.

The measurement concept is based partly on recognition that there is a distribution of velocities of food particles within a pumped food stream. If the shortest time of transit of any particle in a statistically representative group of particles between two measurement locations along the pipe exceeded the minimum time needed to accomplish sterilization at the temperature of the stream, then the food in the stream could be assumed to be sterilized. Both maximum and mean velocities can also be obtained from the measurements to prevent overcooking.

As shown in Figure 1, two pairs of microwave transducers would be used; one at the upstream and one at the downstream measurement location. At both locations, the pipe (or at least transducer windows built into the pipe) would have to be transparent to microwaves. Each transducer pair would comprise a microwave transmitting antenna, a microwave receiving antenna, and impedance-matching dielectric blocks fitted to the pipe. The food particles for use in the measurements would be marked (that is, made to respond to microwaves in a distinct manner) by inserting small pellets of low-density metal, dipoles resonant at the microwave frequency, or diodes (to generate harmonics).

The marked particles would be injected into the food stream somewhere upstream of the upstream measurement

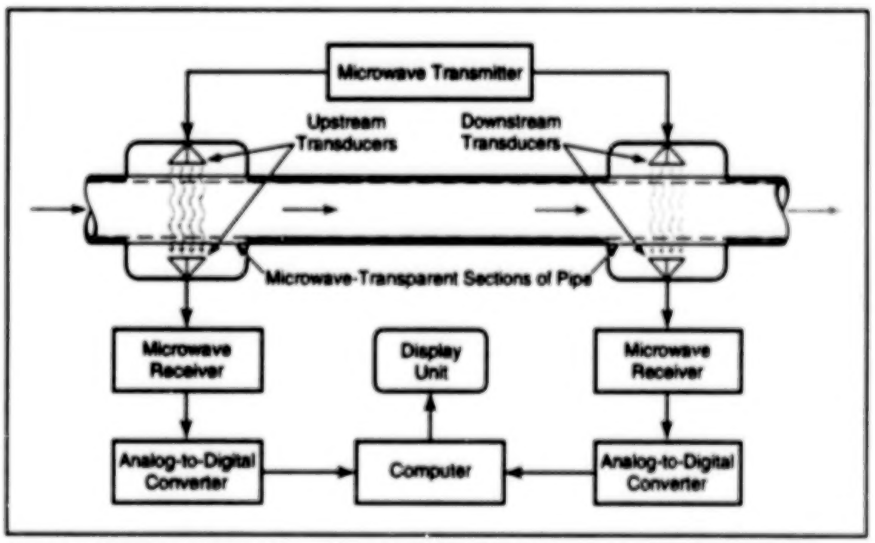

Figure 1. Microwave Transducers Would Detect the passage of marked food particles.

location. As the marked particles passed the upstream measurement location, characteristic signal peaks or valleys (e.g., increases or decreases in reflected or transmitted power, changes in phase, or generation of harmonics) would be detected via the upstream pair of transducers. Similar peaks or valleys, delayed by transit times and spread out because of the distribution of velocities, would be detected when the particles passed by the downstream pair of transducers (see Figure 2). The time between the last peak or valley detected by the upstream transducers and the first peak or valley detected by the downstream transducers would be deemed to be the minimum transit time of any particle in the stream.

This work was done by G. D. Arndt of **Johnson Space Center** *and J. R. Carl of Lockheed Engineering and Sciences Co. Further information is contained in a TSP [see page 1].*

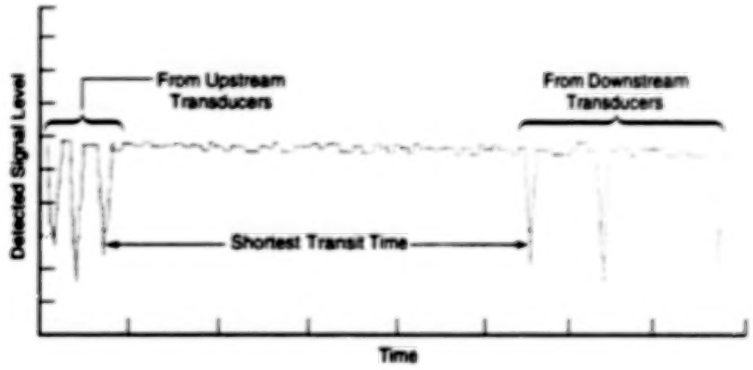

Figure 2. Times Between Characteristic Signals generated during passage of marked particles by the upstream and downstream transducers would be measured. For the purpose of ensuring sterilization, the shortest measured transit time would be taken to indicate the minimum time spent by any particle at the temperature of the stream.

This invention is owned by NASA, and a patent application has been filed. Inquiries concerning nonexclusive or exclusive license for its commercial development should be addressed to the Patent Counsel, Johnson Space Center [see page 1]. Refer to MSC-22451.

Automated Testing of Solar Photovoltaic Arrays

Time-consuming, error-prone manual testing is no longer necessary.

NASA's Jet Propulsion Laboratory, Pasadena, California

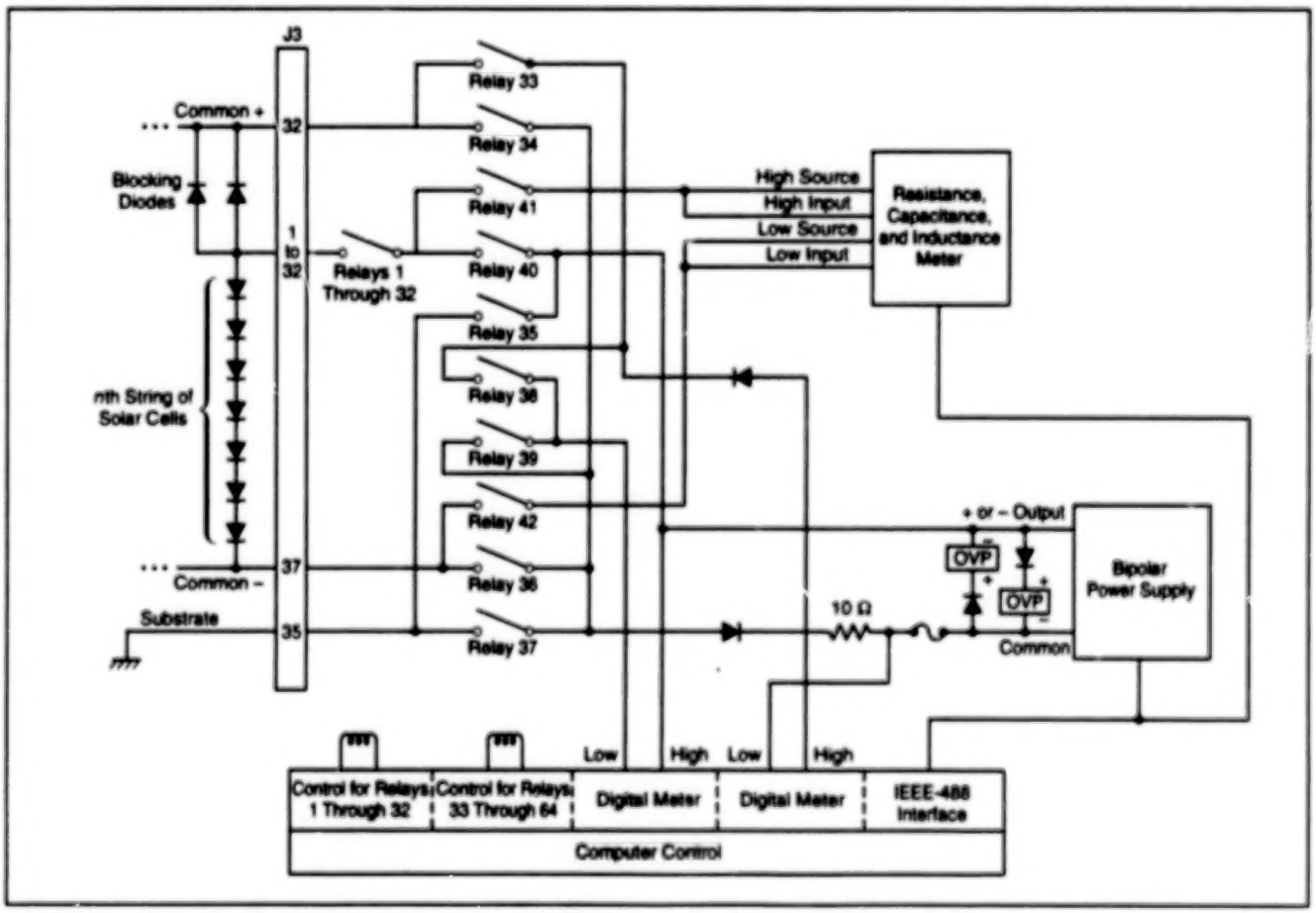

The Test Hardware, operating under computer control, automatically measures electrical parameters of strings of solar cells in an array. For safety, the power supply includes crowbar circuitry, a fuse in common output line, blocking diodes for reversal of voltage, and current and voltage limiting.

A system of computer-controlled electronic test equipment has been developed to automate the electrical testing of arrays of solar photovoltaic cells. The system, called the "Solar Array Ground Support Equipment Testbed" (SAGSET), was designed specifically for diagnosis of solar arrays on spacecraft, and can readily be adapted to use on terrestrial solar arrays. In comparison with manual testing, the use of the SAGSET is easier and more accurate, and takes about one-fifth as much time.

The SAGSET includes test hardware (see figure), a control computer, and software that is executed on the computer to control a selected test. The computer accepts, as input, the specifications of the array. Then the computer controls the testing consistent with the specifications; logging measurement data while generating a display of pass/fail condition, test-equipment activity, and the identity of the string of cells being tested. This appears to be the first computer-controlled, automated diagnostic system capable of testing individual strings of solar photovoltaic cells within arrays.

At the stage of development when the information was reported for this article, the SAGSET was capable of performing the following tests:

- *Bus Isolation* — Determine whether the + and – panel buses are isolated from the substrate by more than 5 MΩ.
- *String Isolation* — Determine whether each string in the array is isolated from the substrate by more than 5 MΩ.
- *Diode Forward Conductance* — Determine whether each pair of blocking diodes conducts with a potential drop of about 0.7 V.
- *Diode Reverse Leakage* — Determine whether each pair of blocking diodes has leakage current of < 1 μA.
- *String Continuity* — Determine whether, in the dark, each string of cells conducts at about 20 percent of short-circuit current when a potential of about 0.9 V × the number of cells is applied to the string.
- *String Capacitance* — Determine whether, in the dark, the capacitance of each string of cells is within ±1 percent of the baseline capacitance (nominally 25 nF for a 40-cell string in the original spacecraft application). The system is required to detect a decrease of 0.83 percent in the capacitance of a string; in the case of the 40-cell string of the original application, this is equivalent to being capable of detecting the loss of 1/4 of one cell.

After further development, the SAGSET is expected to be able to perform several additional tests, including determination of current-vs.-voltage output curves of illuminated strings.

This work was done by Dale R. Burger, Robert L. Mueller, Chris Evans, and Hung Ta of Caltech for **NASA's Jet Propulsion Laboratory**. *Further information is contained in a TSP [see page 1].*
NPO-19753

Fiber-Optic Data Bus for a Sensor Network

A tokenless protocol would ensure efficient transmission from high-speed sensors.

NASA's Jet Propulsion Laboratory, Pasadena, California

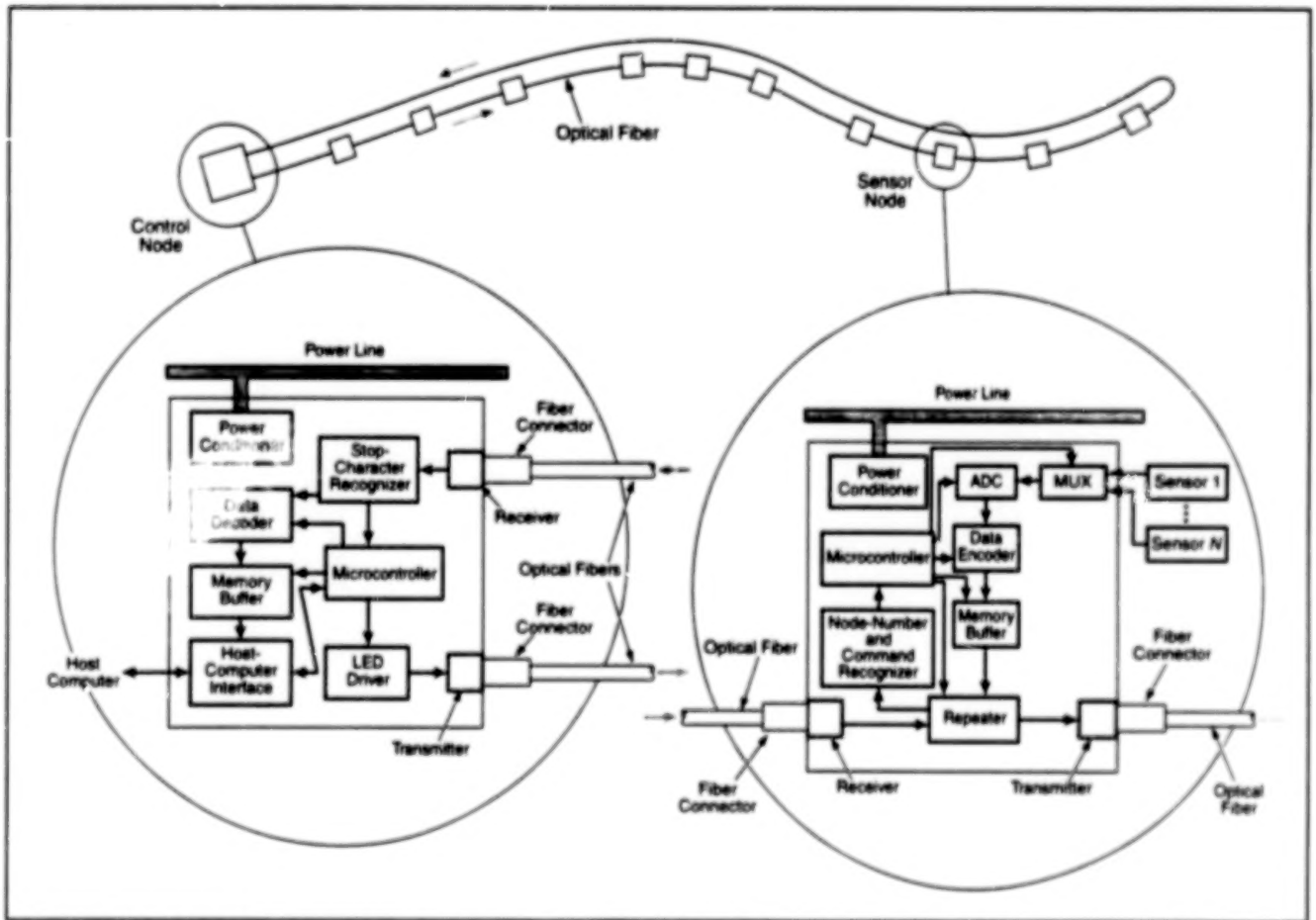

The Fiber-Optic Data Bus for Sensors would comprise sensor nodes connected to each other in series and to a control node via a fiber-optic ring. Each sensor node would contain an analog-to-digital converter (ADC), a multiplexer (MUX) for combining signals from several sensors, and a light-emitting-diode transmitter (TX), and an optical receiver (RX). Electrical power would be supplied on a line separate from the fiber-optic data line.

A proposed fiber-optic data bus would connect a network of high-data-rate sensors to a host computer. The bus could, for example, carry signals from multiple acoustic-emission sensors or video cameras, which generate data at rates greater than 10 Mb/s. The bus could be adapted for use in diverse systems that include many widely distributed sensors; e.g., structural-monitoring systems in aircraft, buildings, and bridges, and traffic-monitoring systems. It would cost less than does a point-to-point bus in which each sensor is connected to the host computer by an individual link. The bus would also carry data at rates much greater than those of wire buses in conventional local-area networks for computers.

The bus would link the sensors in a daisy-chain configuration; the bus would comprise a control node and many sensor nodes joined together in a unidirectional fiber-optic ring (see figure). The bus could be modified quickly by addition or deletion of sensors of various types. For efficient transmission of sensor data, the bus would use a tokenless, noncontention protocol for accepting data from individual sensor nodes. It would automatically assign addresses to the nodes by numbering them in simple numerical sequence in a stimulus/response numbering procedure at the beginning of operation; thus, addresses would be automatically reassigned when the bus was turned on after nodes were added, removed, or became inoperative.

The control node would communicate with the host computer and would control some of the activities of the sensor nodes. The sensor nodes would digitize the sensor outputs and send them to the control node according to the protocol. Each sensor node would contain a single integrated-circuit chip. The chip could be made very compact by incorporating the analog-to-digital converter circuitry with the rest of the circuitry in such a way that the input/output lines on the chip would carry data in serial mode.

After the control node had numbered the sensor nodes, the bus would be ready for acquisition of sensory data by the control node. Starting from node 1, each node would send data through a repeater in the following node, following in numerical sequence until the last node transmitted the data to the control node. The sequence would be implemented as follows: After each node finished sending its data, it would send a "stop" character. Each node would count the number of "stop" characters it had received and would transmit when its turn came. Thus, node 2 would transmit after receiving the single "stop" character from node 1, node 3 would transmit after receiving the two "stop" characters from nodes 1 and 2, and so forth. Alternatively, the control node could direct a single-send command to a specific node, which would then send its data and relinquish control to the control node when it had finished.

The maximum transmission time allowed for a sensor node would be programmable by the control node. If a sensor node did not respond after a brief interval — say 5 ms — it would be considered dead, and the control node would drop it from the numbering scheme and reassign numbers to the remaining nodes.

This work was done by Duncan T. H. Liu of Caltech for **NASA's Jet Propulsion Laboratory**. *Further information is contained in a TSP [see page 1].*
NPO-19712

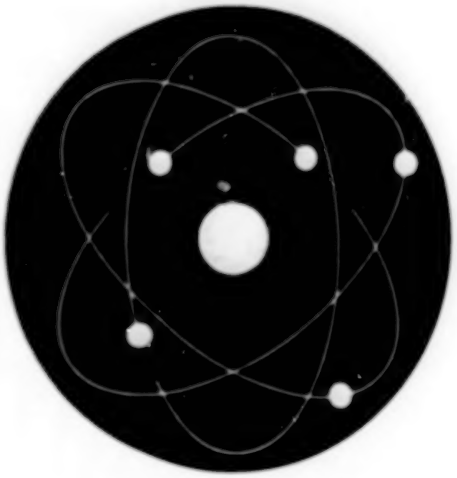

Physical Sciences

Hardware, Techniques, and Processes

29 Transient Thermal Testing of a Flight-Test Article

Transient Thermal Testing of a Flight-Test Article

Controlled radiant heating in a laboratory simulates in-flight thermal conditions.

Dryden Flight Research Center, Edwards, California

A method of controlled radiant heating enables laboratory simulation of the transient aerodynamic heating that occurs on a flight-test article during high-speed flight. In the original application for which this method was devised, the flight-test article was a device called a "wing glove." This device was designed to be mounted on the wing of an air-launched spacecraft-booster rocket to obtain data on cross-flow boundary-layer transition in the speed range of mach 6 to 8. The glove was designed to maintain a specific aerodynamic shape during the extreme aerodynamic heating encountered along the trajectory of the booster rocket.

Ground tests were required to be performed to simulate the flight of the booster rocket from the drop conditions of approximately mach 0.8 at an altitude of 40,000 ft (12 km), through first-stage burnout at approximately mach 8 at 200,000 ft (61 km). These conditions translated into temperatures on the glove ranging from –30 °F (–34 °C) at launch to 500 °F (260 °C) at first-stage burnout. New laboratory test techniques that, together, constitute the present controlled-radiant-heating technique were developed to enable simulation of the thermal conditions encountered in flight (see figures).

The design of the glove posed some testing problems that were solved by the development of these techniques. The glove included a thick leading edge plus relatively thin upper and lower skins. The thick leading edge acts as a heat sink. The large variation in the thickness of the glove material and structure presented the most significant challenge in the laboratory application of heating loads. Although closed-loop temperature control produced acceptable results on the thin-skin portion of the glove, difficulties were encountered while attempting to utilize closed-loop temperature control on the thick leading edge. The thickness of the leading edge and the nonuniform thermal gradients required at the leading edge produced a set of conditions well outside the control envelope of the system used for closed-loop temperature control.

Accordingly, an important element of the present method is a technique for programming the temperature-control system to follow prescribed heat-flux profiles in an open-loop mode. A test was performed at

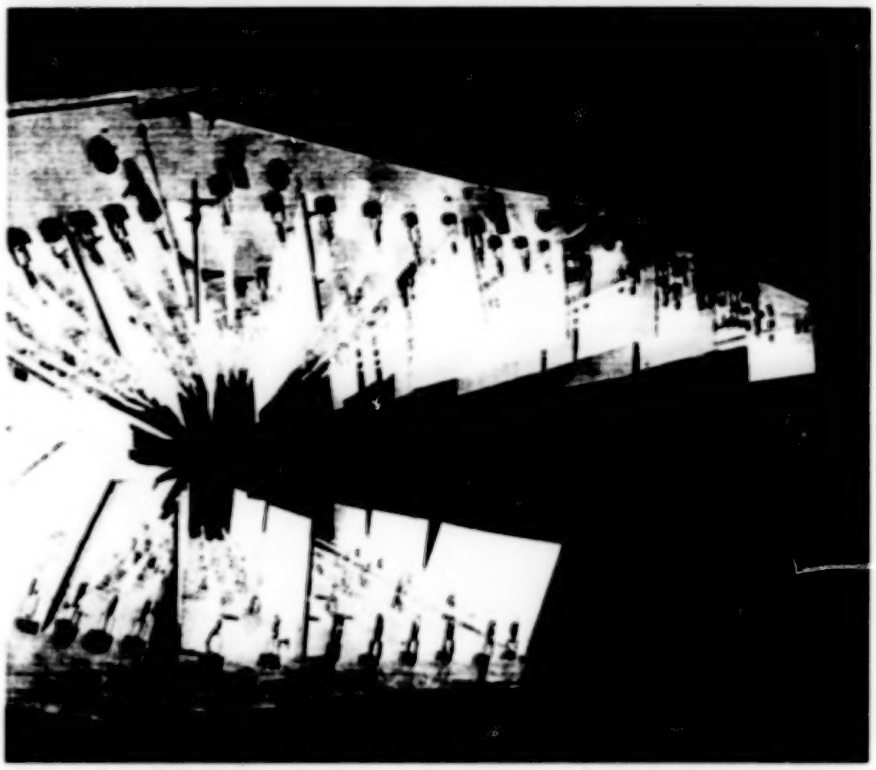

Figure 1. A Radiant Heater in the Flight Loads Laboratory at Dryden Flight Research Center contains 234 heat lamps attached to stainless-steel reflectors and divided into 39 temperature-control zones.

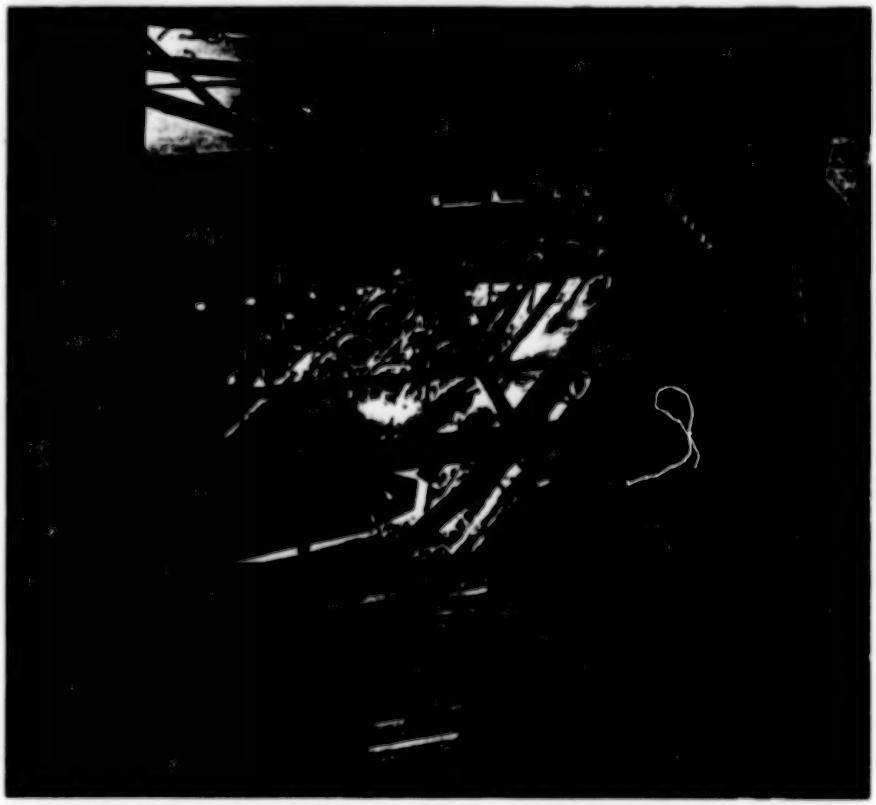

Figure 2. The Radiant Heater Is Shown in Use in a radiant-heating test. The heater produced heat fluxes up to 30 Btu/(ft²·s) (3.4 × 10⁵ W/m²) in the most brightly lit areas.

a constant power level to obtain a calibration for heat flux per power level. Predicted flight heat fluxes as functions of time could then be turned into heating-power levels as functions of time. These power-level histories were entered into the temperature-control-system computer and used to run transient thermal tests. The measured and desired temperature-vs.-time history for each test could then be used to adjust the heat-flux profiles by the following equation:

$$\Delta q(t) = \rho C_p \tau \left(\frac{\Delta T^p(\Delta t)}{\Delta t} - \frac{\Delta T^m(\Delta t)}{\Delta t} \right)$$

where

Δq = differential heat flux,
t = time,
ρ = mass density of material,
C_p = specific heat of material,
τ = nominal thickness,
T = temperature

$\frac{\Delta T^p(\Delta t)}{\Delta t}$ = slope of the predicted temperature-vs.-time profile, and

$\frac{\Delta T^m(\Delta t)}{\Delta t}$ = slope of the measured temperature-vs.-time profile.

The differential heat flux was calculated from this equation (using an experimentally adjusted thickness τ). A new power-level command profile would be determined, and the transient test would be run again. Generally, one or two iterations produced acceptable results.

This testing method made it possible to obtain measured temperature-vs.-time profiles acceptably close to the desired profiles. Results of tests indicated that closed-loop control yielded errors of the order of ±5 °F (±2.8 °C) on the thin-skin areas of the glove. The open-loop technique was found to yield temperatures within about ±20 °F (±11 °C) of the desired profiles, satisfying program requirements.

This work was done by Thomas J. Horn and W. Lance Richards for **Dryden Flight Research Center**. *Further information is contained in a TSP [see page 1].*
DRC-96-45

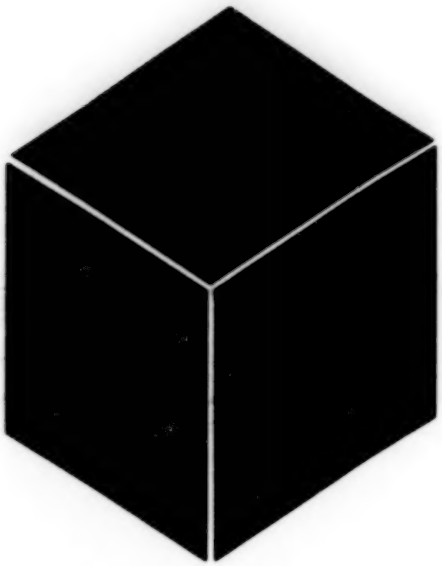

Materials

Hardware, Techniques, and Processes

33 Making Pure Oxide Powders
33 Alloys for Electrodes and Catalysts for Reduction of Oxygen
34 Epitaxial Growth of 2H Silicon Carbide
35 Diamond Coats for Electrodes in Ion Accelerators

PLATE PAGE

Making Pure Oxide Powders

Rods are burned in pure oxygen.

Lyndon B. Johnson Space Center, Houston, Texas

The figure illustrates a combustion chamber for making a powdered oxide (usually of a metal) in a single process step. A rod of the metal or other material is mounted vertically in the chamber, and an electrical igniter is placed at its lower end. The chamber is sealed and filled with oxygen at a suitable pressure, which could be as much as 10^4 psig (about 70 MPa). The igniter is then energized, and the rod burns in the oxygen atmosphere. When combustion is completed, the chamber is vented. The oxide produced in the combustion is removed and sized by screening or another suitable procedure. The chamber was tested by using it to make vanadium, silicon, molybdenum, and tungsten oxides.

The purity of the oxides produced in the chamber can be monitored and controlled via analysis of the rods and of the oxygen gas used in the chamber. Variation of the parameters of the combustion process would probably change the shapes and the distribution of sizes of the oxide particles produced.

One proposed modification of the chamber would be the addition of a device to feed a metal rod continuously into the chamber during combustion. This modification would make it possible to produce large batches of oxide powder with minimum opening and closing of the chamber. In the cases of metals and metal alloys that burn at atmospheric pressure, a continuous-oxide-removal subsystem might also be used, so that the chamber could operate continuously.

This work was done by Joel M. Stoltzfus of **Johnson Space Center** *and Subhasish Sircar of Lockheed Engineering and Sciences Co. Further information is contained in a TSP [see page 1].*

This invention is owned by NASA, and a patent application has been filed. Inquiries concerning nonexclusive or exclusive license for its commercial development should be addressed to the Patent Counsel, Johnson Space Center [see page 1]. Refer to MSC-22358.

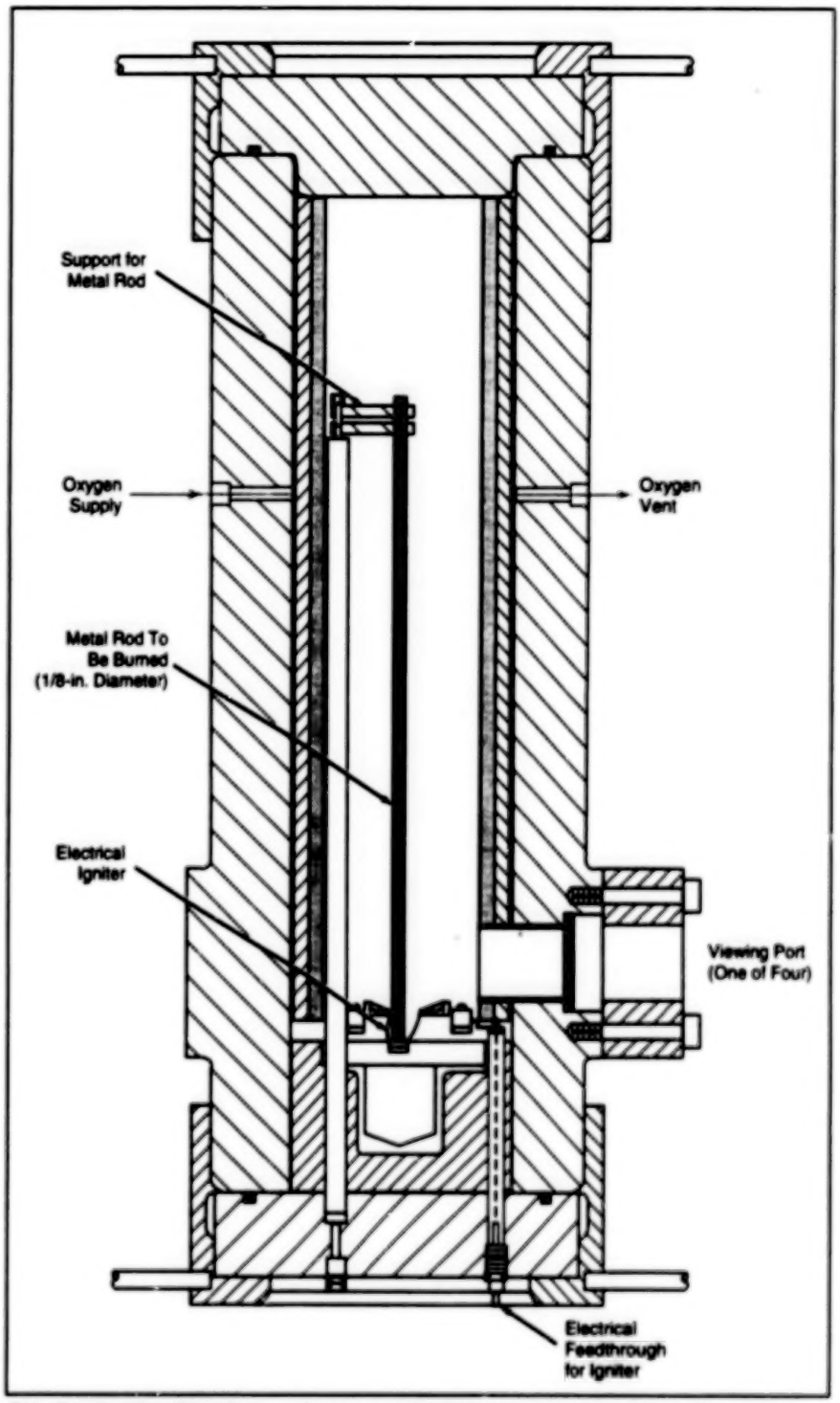

This Combustion Chamber produces a metal oxide by burning the metal rod in oxygen.

Alloys for Electrodes and Catalysts for Reduction of Oxygen

Mixtures of lanthanides could catalyze reduction of oxygen in electrochemical cells.

NASA's Jet Propulsion Laboratory, Pasadena, California

Selected intermetallic compounds of lanthanum and other alloy mixtures of lanthanides have been identified as possible options to replace the expensive noble-metal catalysts used for the reduction-of-oxygen reactions in alkaline primary and rechargeable cells and fuel cells. The resulting fuel cells and batteries could be used in electric vehicles, load leveling, and

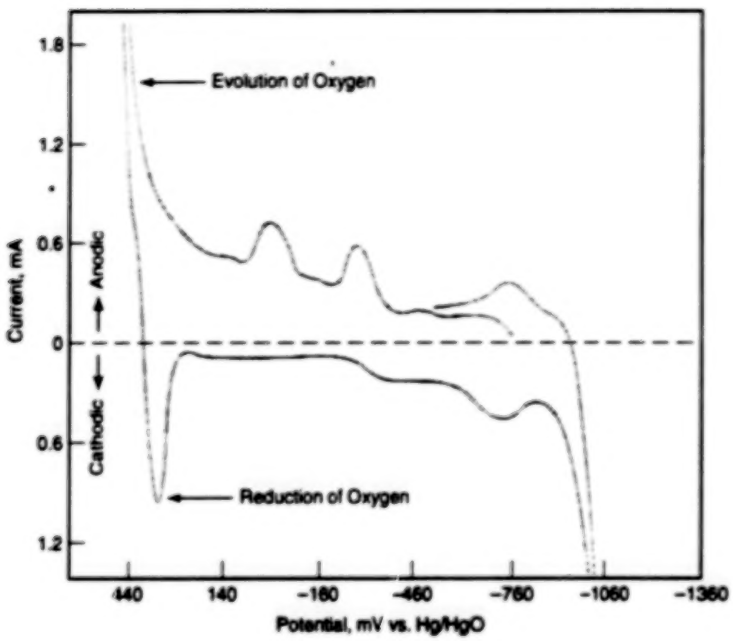

This Cyclic Voltammogram was plotted from measurements on an MH electrode with an area of ~0.12 cm^2 in 6 M KOH electrolyte.

other applications in which high energy densities and power densities are required.

The electrochemical reduction of oxygen is well utilized as the cathodic reaction (at the positive electrode) in a metal/air cell or fuel cell. Because of the peculiarities of the chemical kinetics at the surfaces of typical electrode materials used for this purpose, the reaction is usually slow, giving rise to the need for a catalyst to accelerate the reaction. The alloys of the metals mentioned above (which are also known as rare-earth and transition metals) were selected as candidate replacement catalysts partly because they can undergo electrochemical hydriding and dehydriding at high negative potentials and can absorb significant amounts of hydrogen; these capabilities are amenable to high energy densities.

These alloys are designated collectively as "metal hydride" (MH) alloys, although a more precise name might be "metal-hydride-forming alloys." Two classes of MH alloys are used in the advanced alkaline rechargeable cells known as nickel/metal hydride (Ni/MH) cells. One of these classes comprises alloys of V, Ni, and Cr; the other class comprises alloys of La, Ce, Pr, Nd, Ni, Co, Mn, and Al. An important characteristic of MH alloys is that electrochemical reduction of oxygen can take place on their surfaces: this characteristic would enable an Ni/MH cell to operate while hermetically sealed, especially in positive-limited design. The oxygen evolved at the NiOOH electrode (the positive electrode) in such a cell is continuously reduced on the MH electrode, thus providing an overcharge capability for the cell. An MH electrode can function as an electrocatalyst for the reduction-of-oxygen reaction as well as for the hydrogen-ionization reaction, so that it can be used as a bipolar electrode in a regenerative fuel cell.

To verify the feasibility of the electrochemical reduction of oxygen on MH electrodes, cyclic voltammetric experiments were performed on MH electrodes in alkaline electrolyte solutions. Each experimental MH electrode was subjected to an initial anodic scan (oxidation) to a potential of 0.4 V vs. Hg/HgO [or −0.5 V vs. standard hydrogen electrode (SHE)] before the absorption of hydrogen. The interference caused by dehydriding of the MH electrode was thus eliminated. The cyclic voltammetric peaks in this region would correspond either to the oxidation of the elements of the MH or to the reactions involving electrolyte. Subsequently, the electrode was subjected to a reverse (cathodic) scan to examine the reduction of oxygen or any oxidized species evolved or desorbed at the surface of, or from within, the MH alloy.

The figure shows a typical voltammogram from such an experiment. In this case, the voltammogram includes two or three small peaks around 50 mV and a large peak at 400 mV. The small peaks are attributed to the dissolved oxygen, inasmuch as all the metallic constituents of the MH alloy are apparently oxidized, even at the open-circuit potential of −500 mV. Only manganese can undergo oxidation to a high-valence oxide in this range. The peak around 400 mV is related to the evolution of oxygen at the MH electrode. In the subsequent reduction scan, a strong peak is observed at 350 mV, which may be assigned to the reduction of the oxygen either dissolved in the electrolyte or evolved in the preceding anodic scan. It is therefore clear that the reduction of oxygen as well as evolution of oxygen can occur readily on the MH electrode.

This work was done by Ratnakumar V. Bugga and Gerald Halpert of Caltech for **NASA's Jet Propulsion Laboratory**. *Further information is contained in a TSP [see page 1].*

In accordance with Public Law 96-517, the contractor has elected to retain title to this invention. Inquiries concerning rights for its commercial use should be addressed to

William T. Callaghan, Manager
Technology Commercialization
JPL-301-350
4800 Oak Grove Drive
Pasadena, CA 91109

Refer to NPO-19282, volume and number of this NASA Tech Briefs *issue, and the page number.*

Epitaxial Growth of 2H Silicon Carbide

Applications could include high-temperature, high-frequency electronics and ultraviolet laser diodes.

Lewis Research Center, Cleveland, Ohio

A thin film of 2H silicon carbide has been grown on a 6H silicon carbide substrate by use of a laser ablation technique. This achievement raises the prospect of further development of advanced electronic, optoelectronic, and electro-optical devices based on SiC.

Some background information will enhance the appreciation of this achievement. Silicon carbide is a large-band-gap semiconductor with high physical and chemical stability at temperatures in excess of 1,000 °C. It occurs in more than 100 different crystalline structures called "polytypes," each of which involves

a unique stacking of two variants of a basic tetrahedral SiC unit along the *c* axis. Each polytype exhibits either a cubic (C), a hexagonal (H), or a rhombohedral (R) symmetry. Each polytype is denoted by a number and a letter (e.g., 3C or 2H); the number denotes the number of tetrahedrons in the unit cell of the crystalline structure, and the letter denotes the symmetry type. The band gaps in these polytypes range from 2.39 eV in the case of 3C SiC to 3.3 eV in the case of 2H SiC.

Silicon carbide in bulk form is usually grown by a sublimation technique. Single-phase crystals of the 4H, 6H, and 15R polytypes of SiC have been grown by this technique. Single-crystal epitaxial films of the 6H and 3C polytypes have been grown by chemical vapor deposition and by molecular-beam epitaxy on both single-crystal silicon and silicon carbide substrates. W. F. Klippenberg suggested in 1963 that 2H SiC should be the stable equilibrium phase in the temperature range of 1,300 to 1,600 °C, but until now, 2H SiC was produced only in the form of small whisker crystals.

The experiment in which the thin film of 2H SiC was grown was performed in a high-vacuum chamber at a pressure of about 10^{-6} torr (about 10^{-4} Pa). The 6H SiC substrate on which the film was to be deposited was heated to a temperature of about 1,300 °C. A KrF excimer laser operating at a wavelength of 248 nm and 2 pulses per second was focused onto a target made of polycrystalline 3C SiC, causing a plasma to emanate from the target. The center of this plasma was directed toward the center of the substrate. In this laser ablation process, a layer of 2H SiC approximately 200 nm thick was grown.

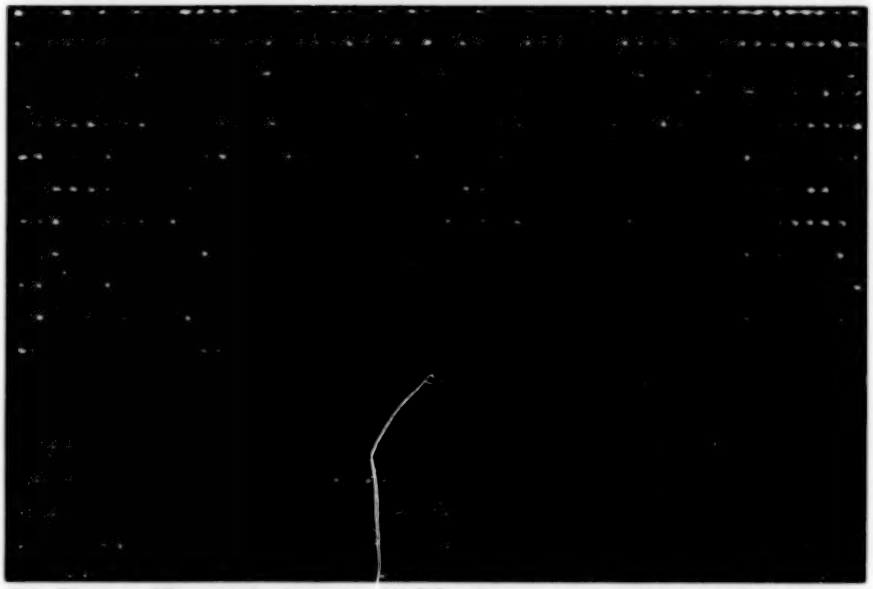

This Electron Micrograph shows two 2H SiC columnar grains and the interface between them. Except for a few faults (especially near the top) wherein small regions have the 3C structure, the grains are relatively free of defects. Notice that at the interface between the grains, the basal planes are nearly continuous.

The polytype of the deposited film was determined by use of electron diffraction and transmission electron microscopy of a cross-sectional specimen prepared by the standard sandwich technique. The figure shows a high-magnification, high-resolution electron micrograph of two columnar 2H SiC grains and the interface between them. The traces of the basal planes are 0.5 nm apart, as marked on the figure.

Potential uses for 2H and other polytypes of SiC include ultraviolet laser diodes, high-speed electronic devices, and high-temperature electronic devices. Because of the difference (0.9 eV) between the band gaps of the 2H and 3C polytypes, it may be possible to fabricate extremely-high-mobility electronic devices with deep quantum wells if epitaxial structures containing sequentially grown 2H and 3C polytypes can be produced.

This work was done by Joseph D. Warner of **Lewis Research Center**, *Martin O. Patton and Mark A. Stan of Kent State University, and Jinwei Yang and Pirouz Pirouz of Case Western Reserve University. Further information is contained in a TSP [see page 1].*
LEW-15988

Diamond Coats for Electrodes in Ion Accelerators

CVD diamond resists erosion better than other electrode materials do.

NASA's Jet Propulsion Laboratory, Pasadena, California

Ion-accelerator electrodes coated with diamond by chemical vapor deposition (CVD) are undergoing development. Ion accelerators include both spacecraft electric thrusters and industrial ion sources. Heretofore, erosion of ion-accelerator electrodes by impacts of charge-exchange ions has degraded performances and limited operational lifetimes. As early as the 1960s, it was known that carbon resists erosion by xenon and krypton ions better than does molybdenum, which is the material of conventional ion-accelerator grids. Therefore, carbon-based electrode materials, including carbon/carbon composites and CVD diamond, have been investigated in efforts to develop better ion-accelerator electrodes. Because of its high thermal conductivity and low coefficient of thermal expansion (see Table 1), diamond has been chosen as the specific form of carbon electrode material for the present development effort.

As part of this effort, experiments were conducted on specimens of molybdenum, a carbon/carbon composite, and CVD diamond. Each specimen was mounted in a vacuum chamber and bombarded with xenon ions at kinetic energies of 500 and 750 eV. The sputter yield and rate of erosion of each specimen at each energy was measured; the CVD diamond specimen was found to undergo the slowest erosion (see Table 2).

Pure diamond is an electrical insulator, but electrodes are required to be electrically conductive. Therefore, it would be necessary to dope the CVD diamond surface layers to make them electrically conductive. Because the electrical current that an ion-accelerator grid must conduct is typically no more than several tens of milliamperes, doping to obtain the required amount of conductivity does not pose a major problem. (Moreover, the effects of resistive heating are minimized by the high thermal conductivity and low thermal expansion.) Experience teaches that p-type doping with boron is most effective, and can be effected by adding the appropriate quantity of diborane to the other

THERMAL CONDUCTIVITY		
Material	Thermal Conductivity, W/(m · K)	Measurement Temperature, °C
Molybdenum	138	20
Carbon/Carbon Composite	830	21
Diamond	2000	20
Copper	401	20

COEFFICIENT OF THERMAL EXPANSION		
Material	Coefficient of Thermal Expansion in Units of 10^{-6}/K	Measurement Temperature, °C
Molybdenum	5.43	527
Carbon/Carbon Composite	−1.5	527
Diamond	3.8	527

Table 1. The **High Thermal Conductivity** of diamond keeps thermal gradients small; this, in combination with a relatively small coefficient of thermal expansion, keeps thermal distortions small, thereby helping to maintain the precise grid shapes needed for high accelerator efficiencies.

Material	Ion Energy = 500eV		Ion Energy = 750eV	
	Sputter Yield[b], Atoms per Ion	Rate of Erosion[b,c] Å/min	Sputter Yield[b], Atoms per Ion	Rate of Erosion[b,c] Å/min
Molybdenum	1.04	6.08	1.27	743
Carbon/Carbon Composite	0.181	83	0.218	98.2
CVD Diamond	0.243	52	0.246	52.5

[a]Base Pressure = $1.1 \cdot 10^{-6}$ torr, Average Density = 2.17 mA/cm^2
[b]Base Pressure = $2.3 \cdot 10^{-6}$ torr, Average Density = 3.43 mA/cm^2
[c]Normalized to a Current Density of 1 mA/cm^2

Table 2. The **Rates of Erosion Under Bombardment by Xenon Ions** were lowest for the CVD diamond specimen; this suggests that CVD diamond coats could extend the operating lives of ion-accelerator grids.

source gases (e.g., methane and/or ethylene diluted with hydrogen) used in CVD of diamond films.

At present, three methods of fabrication of ion-accelerator electrodes with CVD diamond surface layers are under consideration. In the first method, a molybdenum electrode grid would be coated with a CVD diamond film. The adhesion of the CVD diamond film to the molybdenum substrate could be improved by performing the deposition at a temperature favorable to the formation of an intermediate layer of molybdenum carbide and possibly other materials of intermediate composition.

In the second method, a thick diamond film would be deposited on a substrate, then removed from the substrate to produce a freestanding diamond structure. Deposition of films to make freestanding structures is done routinely in the industry, as is laser drilling of holes (which is necessary to form a grid). However, the brittleness of the diamond film could necessitate special handling. In a variation of the second method, a freestanding film with holes would be formed in one process step by CVD onto a silicon substrate with areas destined to contain holes masked by silicon dioxide to retard deposition there. In another variation of the second method, diamond would be deposited on a substrate with holes, but further development of this approach would have to await experiments to assess the extent of growth into the holes.

The third method would involve CVD of diamond on a carbon/carbon grid. The results of preliminary experiments indicate that such deposition is promising. However, given the negative coefficient of thermal expansion of carbon/carbon, it would be necessary to experiment to evaluate the adhesion of the diamond film under thermal cycling.

This work was done by Charles E. Garner, David G. Goodwin, and John Blandino of Caltech for **NASA's Jet Propulsion Laboratory**. *Further information is contained in a TSP [see page 1].*
NPO-19481

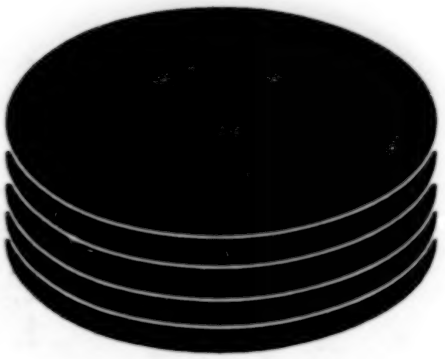

Computer Programs

Electronic Components and Circuits

39 Program Calculates Scattering Parameters of Waveguides

Physical Sciences

39 Program Searches Data Base on Ion/Molecule-Reaction Kinetics

Mathematics and Information Sciences

39 Software for Autonomous Spacecraft Navigation

Computer Programs

These programs may be obtained from COSMIC. Please contact

COSMIC
Computer Services Annex
University of Georgia
Athens, GA 30602
Telephone No. (404) 542-3265.

Electronic Components and Circuits

Program Calculates Scattering Parameters of Waveguides

The WGSPICE computer program, loosely modeled after the circuit-simulation program SPICE, calculates the scattering parameters of a waveguide device or network that comprises a number of fundamental waveguide components connected together. Coded in C++ and using object-oriented principles, WGSPICE calculates the total scattering matrix associated with the complete device out of the more-easily-found scattering matrices associated with the individual components. Such components include rectangular and circular waveguides, junctions between rectangular and/or circular waveguides of different sizes, T and cross junctions, tapers, and terminations. Representations of metadevices (the equivalent of subcircuits in SPICE) can be constructed from component mathematical models and then used multiple times in mathematically modeling an overall device; this feature enables efficient modeling of a device with a periodic structure. Devices that can be modeled include step transformers, filters, diplexers, couplers, smooth or corrugated rectangular or circular horns, and many others. The program is modular, allowing new component models to be added easily. WGSPICE has been implemented on a Sun SPARCstation computer, but could also be run on almost any personal computer, inasmuch as input and output are in ASCII text.

This program was written by Gilbert C. Chinn and Daniel J. Hoppe of Caltech for **NASA's Jet Propulsion Laboratory**. *Further information is contained in a TSP [see page 1].*
NPO-19944

Physical Sciences

Program Searches Data Base on Ion/Molecule-Reaction Kinetics

The Ion Reactions computer program performs searches in a data base on the kinetics of two-body ion/molecule reactions, and prepares reports on the results of the searches. The data base contains more than 10,600 reaction entries compiled from more than 1,000 cited sources in published literature. Searches can be performed with respect to reactants or products and with respect to either ions or neutral atoms; more specifically, the program can search for (1) all reactions for a particular ion, reactant neutral, or reactant pair or (2) all reactant pairs that yield a specified product ion or neutral. This program and the accompanying data base are parts of developmental ion-chemistry software for use by astrophysicists and specialists in planetary atmospheres. In proposed future developments, the data base would be updated, and both the data base and the capabilities of the program would be extended to (1) provide thermochemical data for all reactions and (2) calculate capture rates for all reactions. The present version of the program can be downloaded into either a Macintosh or a DOS format. Proposed future versions of the program and data base would be freely available for downloading via the World Wide Web.

This program was written by Vincent Anicich of Caltech for **NASA's Jet Propulsion Laboratory**. *Further information is contained in a TSP [see page 1].*
NPO-19973

Mathematics and Information Sciences

Software for Autonomous Spacecraft Navigation

Software has been developed to provide for autonomous optical navigation by a spacecraft equipped with one or more video camera(s). The spacecraft in question is that of the New Millennium Deep Space-1 mission to an asteroid and comet, scheduled to begin in mid-1998. The New Millennium navigation system is the first known completely autonomous deep-space navigation system. It relies solely on optical data taken with an onboard camera or cameras and is based largely on optical-navigation techniques that have been proven on the *Voyager* and *Galileo* spacecraft. The major functions performed by the navigation system are picture planning, analyzing image data, determining orbits, designing maneuvers, and generally interacting with other onboard autonomous systems. This spacecraft-based software was developed from ground-based optical-navigation software. It includes novel algorithms for navigating in deep space with only optical data, processing image data, and controlling trajectories. The software functions during all phases of the spacecraft mission: departure, interplanetary cruise, and flyby and/or rendezvous. A prototype of the software has been implemented on a UNIX workstation and has been found to perform well on several mission scenarios.

This program was written by Joseph Riedel, Shyam Bhaskaran, and Stephen P. Synnott of Caltech for **NASA's Jet Propulsion Laboratory**. *Further information is contained in a TSP [see page 1].*
NPO-19939

BLANK PAGE

Mechanics

Hardware, Techniques, and Processes

43 Induced-Strain Actuator With Mechanical Amplification
43 Detecting Delaminations by Use of Piezoelectric Sensors
44 Capture Latch for Assembling Structures
45 Reliable Deployable Strut
45 Tether Mechanism Alleviates Shock Load
46 Gas-Sample-Extraction Valve

BLANK PAGE

Induced-Strain Actuator With Mechanical Amplification

Displacements are multiplied without loss of precise control.

NASA's Jet Propulsion Laboratory, Pasadena, California

An induced-strain actuator has been designed to produce displacements that, albeit small, are larger than those ordinarily produced by such actuators, and to do so without loss of precise control of the displacements. The enlargement of displacements is achieved by use of a two-stage mechanical amplifier.

Induced-strain actuators are mechanisms that include structures that are deliberately made flexible at some points to obtain controlled deflections: a controlled displacement at a designated location in such a structure is produced by enforcing a smaller displacement at another location in the structure, thereby causing the structure to deflect. Induced-strain actuators are typically used to make fine adjustments in the positions and orientations of optical components and instruments.

The present induced-strain actuator contains four smaller input induced-strain actuators that are the sources of the controlled motion. These actuators are coupled to the two-stage mechanical amplifier. The mechanical amplifier includes lever arms that are integral parts of flexure-type structural components (see figure). The four induced-strain actuators connected to the amplifier are preloaded in compression so that vibration does not induce looseness.

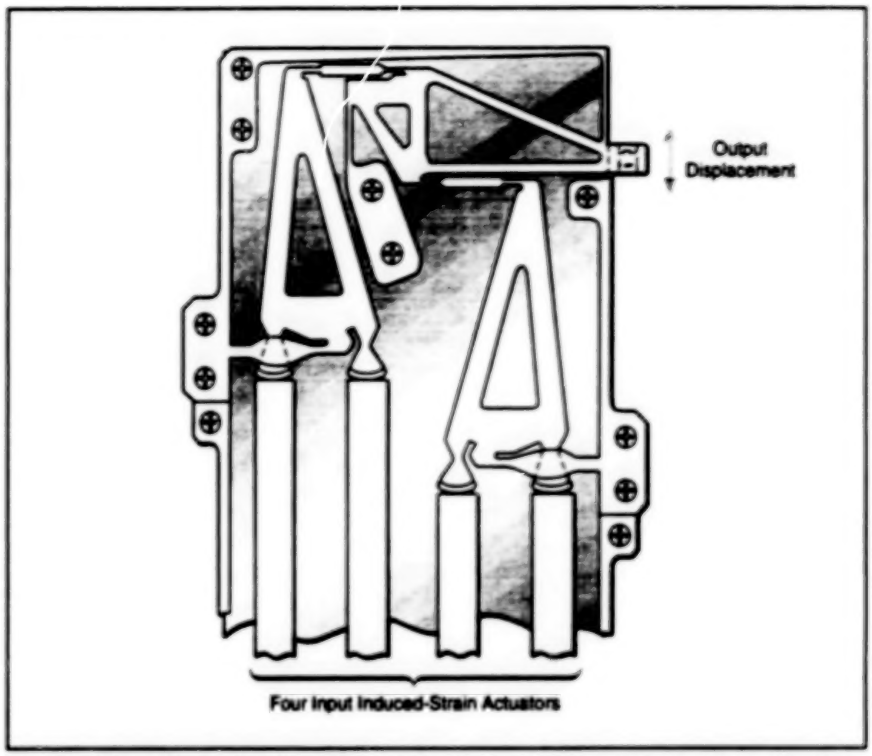

The Two-Stage Mechanical Amplifier includes the two rigid triangular bodies and the flexible connecting narrow strips of material. The output of the mechanical amplifier could be applied to another mechanical amplifier to multiply the displacement further.

This work was done by Robert M. Bamford, Robert J. Glaser, and Donald M. Moore of Caltech for **NASA's Jet Propulsion Laboratory**. *Further information is contained in a TSP [see page 1].*

NPO-19208

Detecting Delaminations by Use of Piezoelectric Sensors

Delaminations would be identified and located via their effects on vibrations.

Lewis Research Center, Cleveland, Ohio

In a proposed method of detecting delaminations in laminated composite-material beams, piezoelectric transducers made of piezoceramic materials would be bonded to the surfaces of the beams (see Figure 1) and/or embedded in internal layers, and would be used to measure vibrations. The vibrations could be excited by external sources or, optionally, by application of driving voltages to some of the transducers. The vibrational responses of the beams as manifested by the output voltages of the sensory transducers would be analyzed for characteristics indicative of the presence (if any), sizes, and locations of delaminations. This method may lead to development of a capability to detect delaminations in real time with minimal instrumentation.

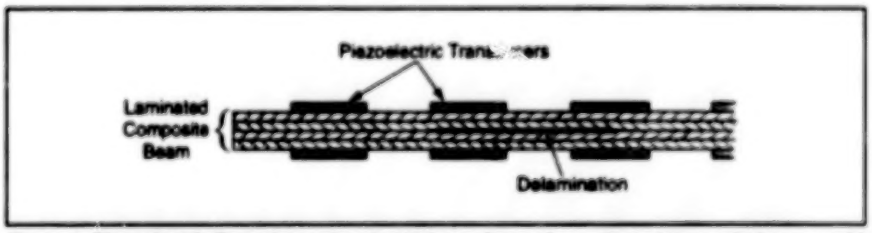

Figure 1. Piezoelectric Transducers bonded to the surfaces of a laminated composite beam would sense (and, optionally, excite) vibrations. The outputs of the sensory transducers could be analyzed to detect the delamination.

The method is analytically demonstrated using a theory that combines the linear theory of elasticity of a laminated composite beam with the linear constitutive relations of the stress, strain, and electric field in a piezoceramic material with anisotropic in-plane elastic properties and a macroscopic polar axis perpendicular to the plane in question. The equations of the combination theory can be solved for both the case of vibroacoustic excitation by an external source

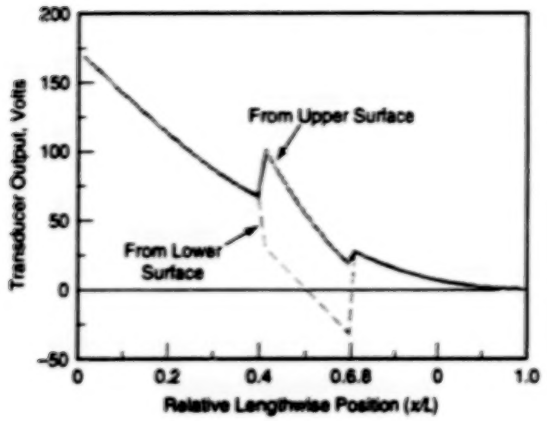

Figure 2. Outputs of Transducers on the upper and lower surfaces of a theoretical cantilever beam of length L with a centrally located delamination of length $L/5$ were calculated as functions of relative lengthwise position (x/L). The central discontinuity in the outputs clearly indicates the position and extent of the delamination.

and the case of vibrations excited locally by some of the transducers.

The solutions can be used to predict output voltages of the vibration-sensing transducers; the voltages predicted for an intact beam differ from those for a beam with delaminations. In particular, in the case of transducers placed at small intervals along a beam at corresponding lengthwise positions on the upper and lower surfaces, the presence of a delamination would be indicated by a discontinuity in the voltage-vs.-position curve derived from the transducer voltages, and by a concomitant difference between the output voltages of the upper- and lower-surface transducers facing each other across a delamination. As shown in Figure 2, a typical plot of such voltages would clearly indicate the position and size of a delamination. Of course, in a practical application, the finite number of transducers and the finite spatial interval between them would limit the precision with which a delamination could be located, but this issue could be addressed by suitable design.

This work was done by Dale A. Hopkins of **Lewis Research Center**, *Dimitrios A. Saravanos of Ohio Aerospace Institute, and Victor Birman of The University of Missouri — Rolla. Further information is contained in a TSP [see page 1].*

Inquiries concerning rights for the commercial use of this invention should be addressed to the Patent Counsel, Lewis Research Center [see page 1]. Refer to LEW-16308.

Capture Latch for Assembling Structures

An improved latch offers a larger-than-usual capture envelope.

Marshall Space Flight Center, Alabama

A capture latch has been proposed for use in assembly of structures in outer space and could also be used in underwater and otherwise hazardous work environments and in remote-control applications. The latch system would consist of three or four latching elements and capture pins spaced around the mating surfaces of two structures to be joined. A latching element mounted on one of two structural members would swing over a capture pin mounted on the other structural member, then pull this other structural member into place. A simple drive screw would actuate the latching element. Torsion springs would soften the mating to prevent damage. The design of this latch would eliminate the need for alignment guides and provide a capture envelope (a range of positions and orientations in which capture could be effected) larger than the capture envelopes of designs now in use. The latch would maintain the alignments of the affected structural members in all axes, protecting any sealing components.

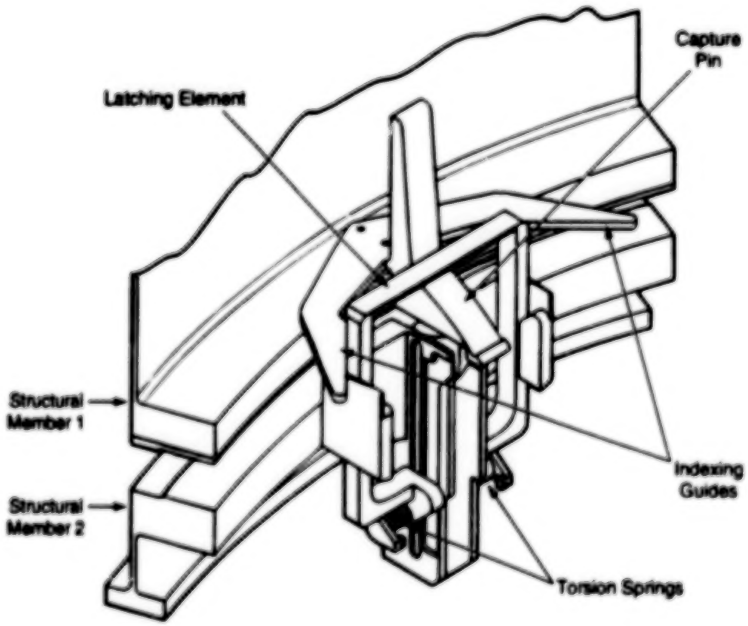

A Latching Element uses indexing guides designed for a large capture envelope. Three or four latching elements are used simultaneously to join the structural members.

This work was done by Charlie VanValkenburgh of Boeing Defense and Space Group for **Marshall Space Flight Center**. *Further information is contained in a TSP [see page 1].*

Inquiries concerning rights for the commercial use of this invention should be addressed to the Patent Counsel, Marshall Space Flight Center [see page 1]. Refer to MFS-28928.

Reliable Deployable Strut

The folded strut unfolds itself upon release.

NASA's Jet Propulsion Laboratory, Pasadena, California

A deployable strut has been designed for simplicity and reliability. The strut contains no sliding parts that could bind during deployment. Intended for one-time deployment, the strut is flexible enough to be foldable nearly in half for stowage pending deployment. When released, the strut unfolds itself.

As shown in the figure, the strut consists of (1) a spring, which is the primary compression member; (2) two thin steel strips, which carry tension, and (3) two end fittings, which form pin-ended attachment points. The tension strips are parts of a one-piece loop that is captured in the two end fittings on the center line of the strut. Once the strut has unfolded itself, it becomes locked straight in the sense that it cannot thereafter be folded except by applying a load in excess of the buckling load.

This work was done by Kenneth Jewett and Jack Frazier of Caltech for **NASA's Jet Propulsion Laboratory**. *Further information is contained in a TSP [see page 1].*
NPO-19957

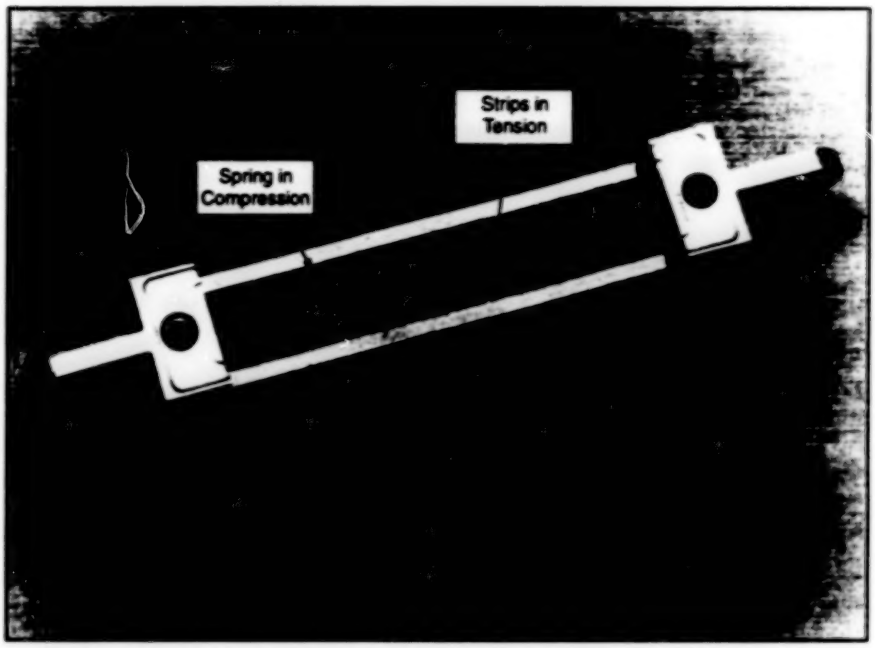

The Spring Pushes on the end fittings, placing the strips in tension.

Tether Mechanism Alleviates Shock Load

A spring and brake help prevent injury to the wearer.

Lyndon B. Johnson Space Center, Houston, Texas

A compact tether mechanism clipped to a waist belt (see figure) alleviates sudden large tensile loads applied to the tether. For example, the wearer can be a mountain climber, firefighter, construction worker, or rescuer tethered by a safety rope, and the mechanism can help to prevent injury to the wearer if the wearer falls and the rope snaps taut.

The mechanism is about 2.5 in. (6.4 cm) in diameter and 4.5 in. (11.4 cm) long. It contains a Kevlar (or equivalent aromatic polyamid) fabric tether 1/2 in. (12.7 mm) wide and 6 ft. (1.8 m) long wound on a spool. A clock spring biases the spool toward retraction of the fabric tether; in this respect, the mechanism resembles a tape-measure mechanism.

The mechanism contains a drag brake that serves as the principal shock-absorbing device. The drag brake includes a pad that remains stationary relative to the spool and a pad that is fixed within the housing of the mechanism. The two pads are pressed together at a preset load. When the tether has been pulled out to a length of about 2 ft. (0.6 m), a clutch engages the stationary pad, causing it to rotate against the fixed pad. This clutch is a one-way clutch; it acts to resist extension of the tether but not to resist retraction. Thus, when the tether is no longer being pulled out by a large load, this clutch disengages the brake, allowing the clock spring to rewind the tether onto the spool.

However, another clutch — a stepped clutch — prevents the spring from rewinding the tether until such time as the wearer is ready. The wearer presses a release button that disengages the stepped clutch, allowing the spring to turn the spool to retract and rewind the tether.

This work was done by Richard D. Smallcombe of Oceaneering Space Systems for **Johnson Space Center**. *Further information is contained in a TSP [see page 1].*
MSC-22468

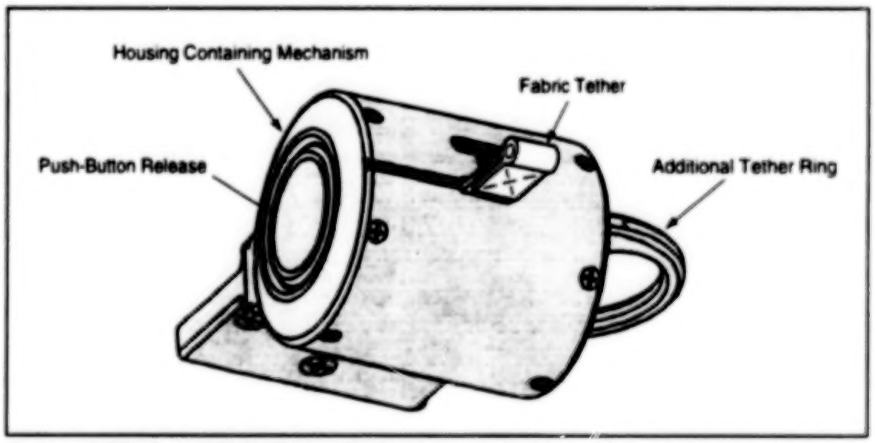

The Load-Alleviating Waist-Tether Mechanism is suited for rescue operations in which sudden falls could cause injury.

Gas-Sample-Extraction Valve

A valve has been designed to be leak-tight and to be used to tap into a fluid line such as on a refrigeration unit. A static seal coupled to a compressible hermetically-sealed metal bellows is used in place of a presently available dynamic O-ring shaft seal, which is prone to leakage. The bellows assembly allows for a controlled depth of penetration into a fluid line to prevent excessive deformation and leakage at the fluid line/valve interface. The valve was designed to tap into shuttle sample cylinders, which utilize copper pinch-off tubes instead of integrated sampling valves. The valve can also be used to add or remove a refrigerant fluid (e.g., Freon) from a refrigeration system, with minimum release of the fluid to the atmosphere.

This work was done by Richard J. Dean and Scott C. Hacker of **Johnson Space Center**. *Further information is contained in a TSP [see page 1].*
MSC-22465

Machinery

Hardware, Techniques, and Processes

49 Staged Regenerative Sorption Heat Pump
50 Heat-Cascading Regenerative Sorption Heat Pumps
51 High-Performance Robotic Vehicle
52 Numerical Simulation of Flow in a Wave Rotor

BLANK PAGE

Staged Regenerative Sorption Heat Pump

Coefficients of performance would be increased by staged compression.

NASA's Jet Propulsion Laboratory, Pasadena, California

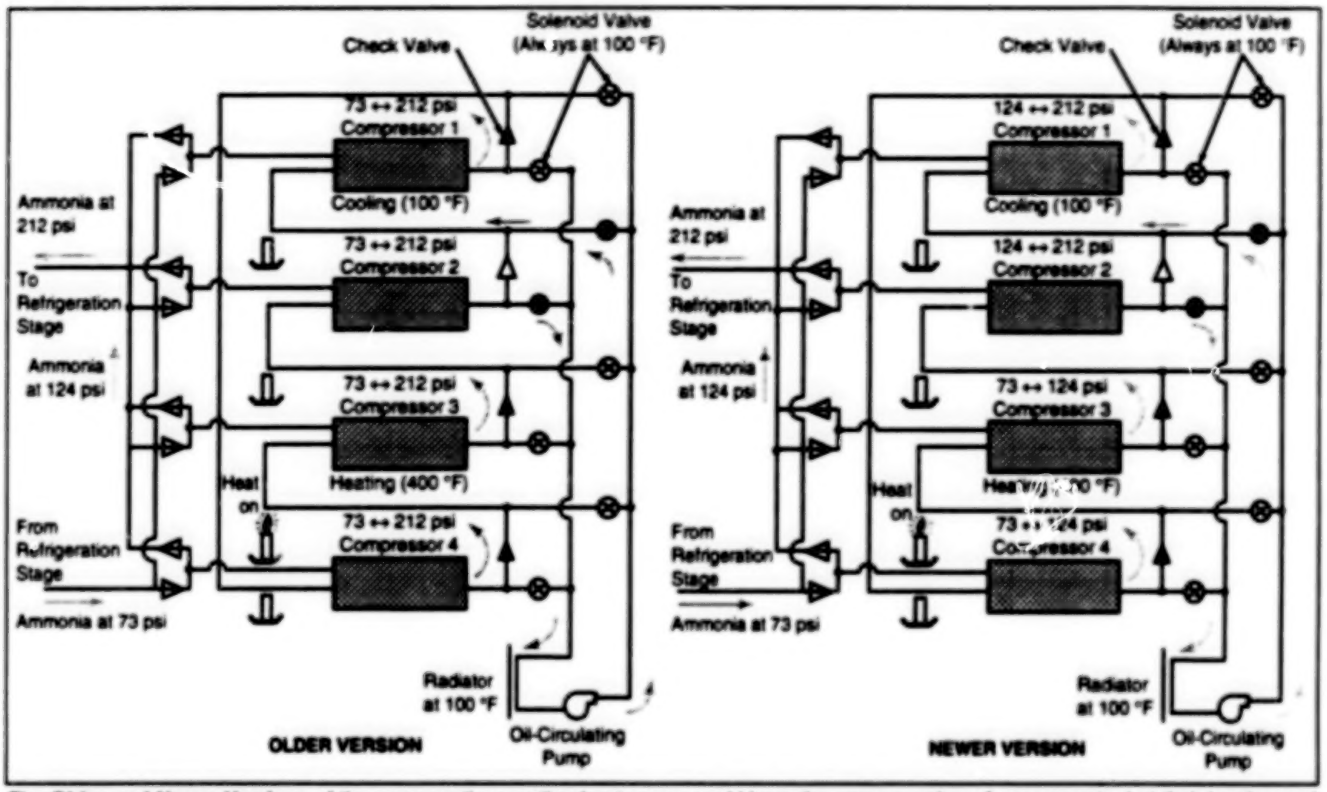

The Older and Newer Versions of the regenerative sorption heat pump would have the same number of components, but their heating and cooling cycles and the switching valves would be timed differently. In the older version, each compressor would operate between the two extremes of pressure; in the newer version, each compressor would effect only one of two stages of compression.

The figure illustrates older and newer versions of a proposed regenerative sorbent-compressor heat pump that could be used to heat or cool a home, office, industrial building, or vehicle. Both versions would operate with non-ozone-depleting, working fluids such as R134a or ammonia. The newer version would offer somewhat greater energy efficiency with minimal added complexity. The basic configuration and principle of operation of the older version are similar, in most respects, to those of the proposed heat pump described in "Improved Regenerative Sorption-Compressor Refrigerator" (NPO-18211), *NASA Tech Briefs*, Vol. 16, No. 8 (August 1992), page 61. There would be four activated-charcoal sorption compressors, which would adsorb a working fluid (in this case, ammonia) when cooled and desorb the working fluid when heated.

Each compressor would be connected to two fluid loops: one containing the ammonia working fluid, the other containing oil, which would be circulated by a pump through all the sorption compressors, through a radiator (for rejection of heat or to supply heat to the inhabited space), and through four internal sources of heat. By appropriate timing of the four internal sources of heat and of solenoid-actuated valves, the oil-circulating loop would pass a cyclic wave of heating and cooling among the four sorption compressors, thereby creating a cyclic wave of sorption and desorption that would cause the working fluid to circulate through an associated refrigeration stage, which is not shown in the figure.

In the older version, the four sorption compressors would be cyclically heated and cooled in sequence, such that each would be cycled between adsorption of ammonia at 73 psi (0.50 MPa) and desorption of ammonia at 212 psi (1.46 MPa). In the newer version, the sorption and desorption would be performed in stages: during one phase of operation, for example, sorption compressors 3 and 4 would act as a first-stage compression subsystem that would operate between 73 psi and 124 psi (0.50 and 0.85 MPa, respectively); sorption compressors 1 and 2 would act as a second-stage compression subsystem that would raise the pressure from 124 to 212 psi (0.85 and 1.46 MPa, respectively).

A cycle could begin with the heating of compressor 3 to desorb ammonia at 124 psi (0.85 MPa) and send it to compressor 1. In the next phase, compressor 2 (which would contain ammonia adsorbed during the preceding cycle) would be heated to desorb ammonia at 212 psi (1.46 MPa) and send it through the refrigeration stage, where it would be expanded to 73 psi (0.50 MPa) to provide cooling at a temperature of 40 °F (about 4 °C). The ammonia returning from the refrigeration stage at 73 psi (0.50 MPa) would be adsorbed by cooled compressor 4. Next, compressor 1 would be heated to desorb ammonia at 212 psi (1.46 MPa), and so on.

The newer version, with its staged compression, would produce about 50 percent more high-pressure ammonia than would the older version for the same expenditure of energy. The coefficient of performance (the cooling or heating power ÷ the power needed to run the heat pump) in cooling would be 1.2 for the newer version (vs. 1.0 for the older version); the coefficient of performance in heating would be 2.2 for the newer version (vs. 2.0 for the older version). The older configuration is being commercialized for home heat pumps and mobile air-conditioners, while the newer configuration is being considered for commercial refrigeration.

This work was done by Jack A. Jones of Caltech for **NASA's Jet Propulsion Laboratory**. *Further information is contained in a TSP [see page 1].*

In accordance with Public Law 96-517, the contractor has elected to retain title to this invention. Inquiries concerning rights for its commercial use should be addressed to

William T. Callaghan, Manager
Technology Commercialization
JPL-301-350
4800 Oak Grove Drive
Pasadena, CA 91109

Refer to NPO-19008, volume and number of this NASA Tech Briefs *issue, and the page number.*

Heat-Cascading Regenerative Sorption Heat Pumps

Heat from hotter chemisorption reactions would energize cooler physisorption or chemisorption reactions.

NASA's Jet Propulsion Laboratory, Pasadena, California

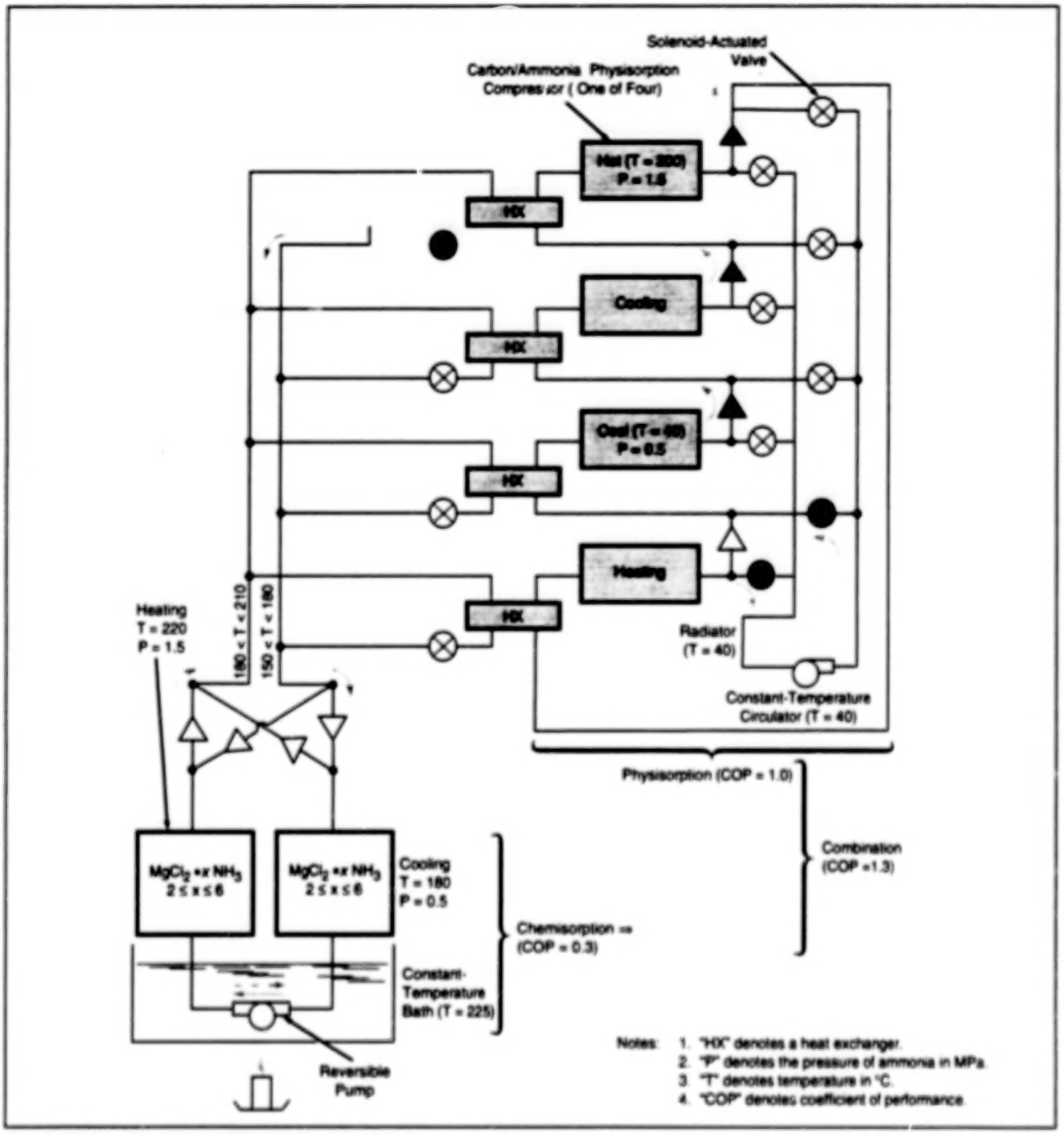
Solenoid-Actuated Valve
Carbon/Ammonia Physisorption Compressor (One of Four)
Hot (T = 200) P = 1.6
HX
Cooling
HX
Cool (T = 60) P = 0.5
HX
Heating
HX
Heating T = 220 P = 1.5
180 < T < 210
150 < T < 180
Radiator (T = 40)
Constant-Temperature Circulator (T = 40)
Physisorption (COP = 1.0)
Combination (COP = 1.3)
$MgCl_2 \cdot x\,NH_3$ $2 \le x \le 6$
$MgCl_2 \cdot x\,NH_3$ $2 \le x \le 6$
Cooling T = 180 P = 0.5
Chemisorption ⇒ (COP = 0.3)
Constant-Temperature Bath (T = 225)
Reversible Pump
Notes:
1. "HX" denotes a heat exchanger.
2. "P" denotes the pressure of ammonia in MPa.
3. "T" denotes temperature in °C.
4. "COP" denotes coefficient of performance.

This **Heat-Cascading Regenerative Sorption Heat Pump** is shown here at one phase of its heating/cooling cycle. Cyclic waves of heating and cooling would be propagated among the four physisorption units by timed control of solenoid-actuated pumps (as in other regenerative sorption heat pumps), accompanied by synchronized reversal of the reversible pump shown at the lower left.

Heat-cascading regenerative sorption heat pumps are conceptually similar to some of the proposed sorption heat pumps reported previously in *NASA Tech Briefs*, except that they would incorporate additional sorption reactions for greater efficiency. One prior non-heat-cascading regenerative sorption heat pump in this line of development was described in "Improved Regenerative Sorbent-compressor Refrigerator" (NPO-18211), *NASA Tech Briefs*, Vol. 16, No. 8 (August 1992), Page 61; another is described in the accompanying article, "Staged Regenerative Sorption Heat Pump" (NPO-19008). Each of these prior conceptual heat pumps is based on physisorption reactions of a single type. However, in a proposed heat-cascading regenerative sorption heat pump, waste heat from a hotter chemisorption reaction would energize a cooler physisorption or chemisorption reaction.

Typically, the working fluid in both the hotter and cooler reactions would be ammonia. The working fluid could be cycled between the same extremes of pressure in both the hotter and cooler reactions (as in a home-heating or home-cooling heat pump). Alternatively, the working fluid in the hotter reaction could be cycled over a wider pressure swing (as in the freezer section of a home refrigerator) while the working fluid in the cooler reaction would be circulated over a narrower pressure swing (to cool the associated refrigerator section).

For example, the heat-cascading heat pump illustrated schematically in the figure would incorporate a hotter chemisorption cycle in which ammonia would be absorbed in magnesium chloride at a temperature of 180 °C and pressure of 0.5 MPa and desorbed from magnesium chloride at a temperature of 220 °C and pressure of 1.5 MPa. A reversible pump would circulate hot oil to the $MgCl_2$ to provide heating. The oil would also pass through one of four heat exchangers, where it would be cooled before cooling the $MgCl_2$ to 180 °C.

In the heat exchanger, heat from the oil would be transferred to the cooler secondary regenerative physisorption cycle, in which ammonia would be desorbed from carbon at 200 °C and 1.5 MPa and absorbed on carbon at 40 °C and 0.5 Pa. Calculations show that with ammonia as the working fluid, heat cascading would increase coefficients of performance by about 30 percent over those of simple regenerative physisorption heat pumps. Similarly, heat cascading combined with staging as described in the accompanying article should yield overall increases of about 50 percent.

This work was done by Jack A. Jones of Caltech for **NASA's Jet Propulsion Laboratory**. *Further information is contained in a TSP [see page 1].*

In accordance with Public Law 96-517, the contractor has elected to retain title to this invention. Inquiries concerning rights for its commercial use should be addressed to

Larry Gilbert, Director
Technology Transfer
California Institute of Technology
Mail Code 315-6
Pasadena, CA 91125
(818) 395-3288

Refer to NPO-19018, volume and number of this NASA Tech Briefs *issue, and the page number.*

High-Performance Robotic Vehicle

The latest model is smaller and more capable than its predecessors.

NASA's Jet Propulsion Laboratory, Pasadena, California

Rocky 7 is the most recent in a series of prototype semiautonomous robotic vehicles that execute tasks with minimal supervision by remote human operators. The vehicles in this series have been called, variously, "rovers" and "microrovers," and have been undergoing development for use in remote scientific exploration of the surface of Mars. They could also be used on Earth in such applications as remote surveillance and routine operations in hostile environments.

Rocky 7 offers the following important performance advantages over its predecessors:

- A computer system containing modern hardware, with software including a real-time operating system;
- A computing environment, provided by both computing hardware and generic software, that is conducive to the development of reconfigurable control software;
- A vision subsystem that includes two stereoscopic pairs of cameras — one forward-looking and one rearward-looking;
- A miniature manipulator for acquiring samples and aiming integrated scientific instruments;
- Fewer locomotion actuators.

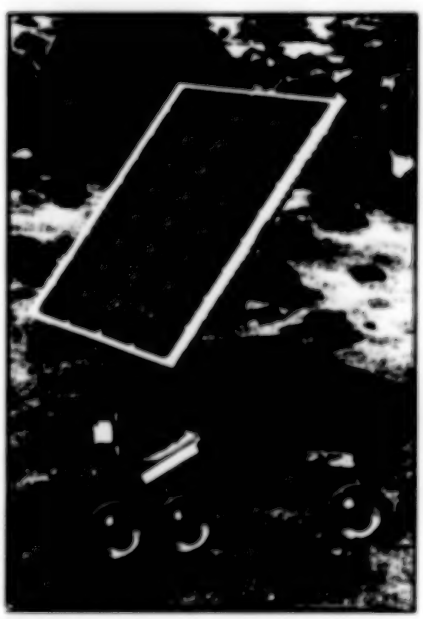

Rocky 7 includes a chassis with dimensions of 41 by 27 by 15 cm. The chassis holds computer hardware, scientific instruments, communication equipment, and power equipment. The total power demand is 48 W, of which the computer system draws 28 W. The total mass of the vehicle is 11.5 kg. The maximum speed of the vehicle is 30 cm/s.

Rocky 7 (see figure) has approximately the same size, mass, and overall number of mechanical degrees of freedom as does a predecessor — the *Pathfinder* microrover, *Sojourner* — but the mechanical degrees of freedom are redistributed to give Rocky 7 greater functionality. The number of degrees of freedom for mobility have been reduced from ten in *Sojourner* to six in Rocky 7; the remaining four degrees of freedom are used in Rocky 7 for the manipulator, which can dig, scoop, point, and grasp.

The software architecture of Rocky 7 facilitates the creation of C++ software modules and the connection of these modules into asynchronous finite-state machines and synchronous data-flow control loops. Asynchronous activities are initiated by a queue of operator commands. Aboard Rocky 7, these commands cause state transitions in one of three state machines: navigation, vision, and manipulation. The image data provided by the forward- and rear-

ward-looking stereoscopic pairs of cameras are used by navigation software to negotiate paths around rocks and other obstacles.

Instead of the flat, fixed solar photovoltaic array like those that powered its predecessors, Rocky 7 includes a solar array that can be turned to face the Sun, maximizing collected power and enabling high-latitude mission scenarios. To further economize on power usage, passive stereo vision is used for obstacle detection, instead of the active laser-stripe triangulation technique used on *Sojourner*.

This work was done by Richard Volpe, J. Balaram, Robert Ivlev, and Timothy Ohm of Caltech for **NASA's Jet Propulsion Laboratory**. *Further information is contained in a TSP [see page 1].*
NPO-19921

Numerical Simulation of Flow in a Wave Rotor

A relatively simple mathematical model accounts for major features of performance.

Lewis Research Center, Cleveland, Ohio

A mathematical model has been developed for use in predicting the performance of a wave rotor. Wave rotors (also called "pressure exchangers") are potentially useful for achieving high overall pressure ratios and peak cycle temperatures in future gas-turbine engines. Shown schematically in Figure 1, a wave rotor is a rotor that contains longitudinal passages. The ends of the passages are alternately opened to stationary upstream ports, closed by stationary upstream and downstream walls, and opened to stationary downstream ports, all by virtue of rotation about a longitudinal axis. The cycle of alternating openings and closings generates unsteady waves in the passages. These waves can be used to transfer energy to and from the working fluid that flows in the passages.

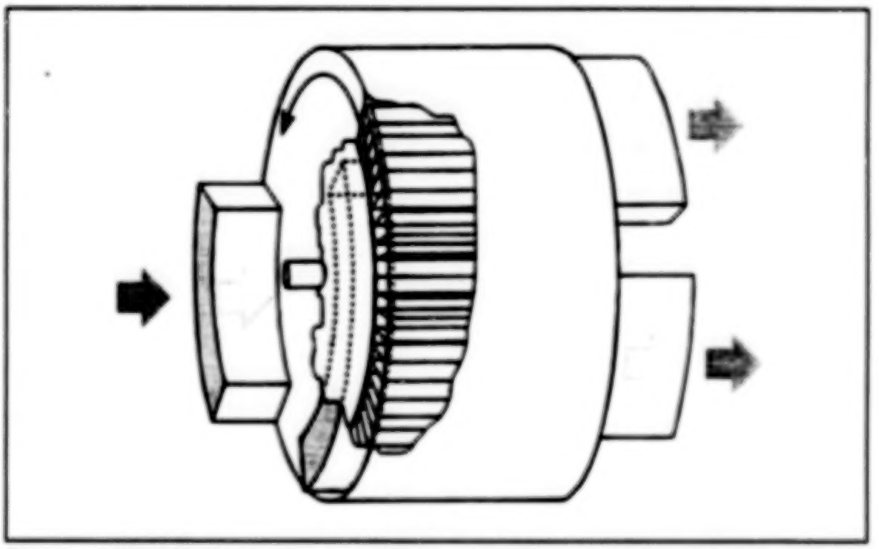

Figure 1. A Wave Rotor provides a combination of switching valve action and wave propagation. With suitable design, it could improve the performance of an advanced gas-turbine engine.

The model is capable of predicting the performance of a wave rotor of specified geometry over a wide range of operating conditions. The model treats the working fluid as a perfect gas that flows in one dimension — along a passage. The equations of the model include source terms that account for the major loss mechanisms of leakage from the ends of the passages, viscosity of the working fluid, transfer of heat from the working fluid to the walls of the passages, finite opening times, shock waves, and nonuniformity of flows through the ports. Because of its one-dimensionality, this model is simple (in comparison with more complicated two- and three-dimensional models) and uses little computer time: this makes it suitable for design as well as analysis.

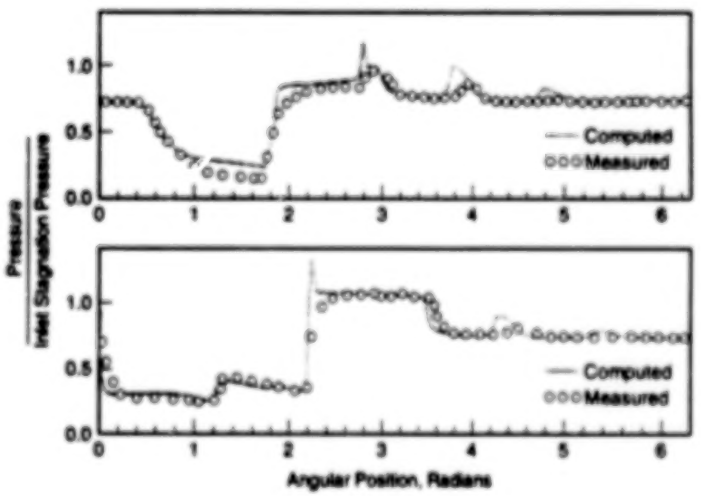

Figure 2. The Relative Pressures at two axial locations in a passage in a wave rotor were predicted and measured as functions of the angle of rotation.

A computer program that implements the model integrates the one-dimensional equations of motion of the gas in a single passage as the rotation moves the ends of the passage across the various ports and walls on the upstream and downstream ends. The ports and walls establish the boundary conditions upon the equations for the flows of mass and heat. Ports are specified in terms of their angular locations relative to a fixed point on the wave rotor, and by representative pressures and temperatures. The computer program accommodates as many as six ports — three on each end. With each time step, Δt, of the numerical integration, the passage advances an increment of angle given by $\Delta\theta = \omega\Delta t$, where ω is the angular speed of rotation.

When the flow is into the passage, the pressure and temperature are interpreted as stagnation values. When the flow is out of the passage, only the port pressure is required, and it is interpreted as

a static value. Because of this directional dependence of the boundary conditions at the ends of the passage, the problem of determining the direction of flow is slightly complicated. The problem is solved by use of an iterative computational procedure that begins with an assumption of outward flow and ends with a recomputation under an assumption of inward flow if the initial assumption of outward flow leads to an inconsistent result. The effects of finite opening times at the ends of the passage are treated by another iterative procedure that also involves initial guesses and recomputation, as needed, to obtain consistent results.

The model was tested by comparing its predictions with measurements taken on three different wave rotors. As shown by the example of Figure 2, the predictions are in substantial agreement with the measurements. The only significant discrepancies that were found lay in the predicted mass flows, which were 10 to 30 percent too high. It is believed that this is due to blockage caused by the finite thickness of the passage walls.

This work was done by Daniel E. Paxson and Gerard E. Welch of **Lewis Research Center** *and Jack Wilson of Sverdrup Technology, Inc. Further information may be found in AIAA-93-0482, "An Improved Numerical Model for Wave Rotor Design and Analysis" and AIAA-93-2522, "A Comparison Between Numerically Modeled and Experimentally measured Loss Mechanisms in Wave Rotors."*

Copies may be purchased [prepayment required] from AEROPLUS, Burlingame, California 94010, Telephone No. (800) 662-2376, Fax No. (415) 259-5047.

LEW-15915

BLANK PAGE

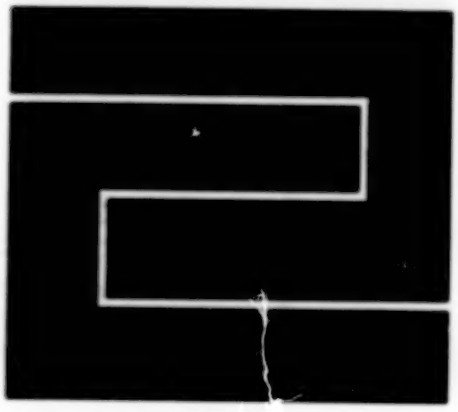

Fabrication Technology

Hardware, Techniques, and Processes

57 Improved Texturing of Surgical Implants for Soft Tissues

58 Ultralight Thermal Radiator

BLANK PAGE

Improved Texturing of Surgical Implants for Soft Tissues

Less labor is needed to prepare mold surfaces.

Lewis Research Center, Cleveland, Ohio

Textured silicone rubber parts for surgical implantation in soft tissues can be made by a process that is improved in that less (in comparison with older processes) labor is needed to obtain the desired surface textures. The textures (typically, microscopic bumps on otherwise smooth surfaces) help to fix the implants in place and to promote the growth of the surrounding tissues in the desired formations.

In general, silicone rubber surgical implants are molded, and the desired surface textures are obtained by correspondingly indenting the mold surfaces prior to molding. Previously, mold surfaces were indented by a variety of labor-intensive and thus expensive fabrication steps. The improved process is less labor-intensive, yet it provides a dense, random distribution of microscopic dents.

The figure illustrates the improved process as it is carried out for a typical two-piece epoxy mold that has been made from a model of the implant. First, the mold is cooled enough to make a thin film of water condense on it from the surrounding air. The wet mold surfaces are dusted with ordinary table salt, some of the crystals of which adhere to the surfaces and become partially dissolved at the points of adhesion. The water film is allowed to evaporate, leaving the sodium chloride crystals clinging to the mold surfaces.

The mold is placed in a vacuum chamber, where a thin film of aluminum is deposited on the mold surfaces and the adhering salt crystals. After deposition, the salt crystals are removed, either by use of a soft brush or by dissolution in water. At this stage, the aluminum film contains pinholes at the former sites of the salt crystals.

The mold is placed in a radio-frequency plasma asher, where atomic oxygen passes through the pinholes and attacks the underlying epoxy (but not the aluminum film), forming hemispherical craters under the aluminum film. When the craters have grown large enough (typically, about 400 μm in diameter), the mold is removed from the asher and the aluminum film is etched away chemically.

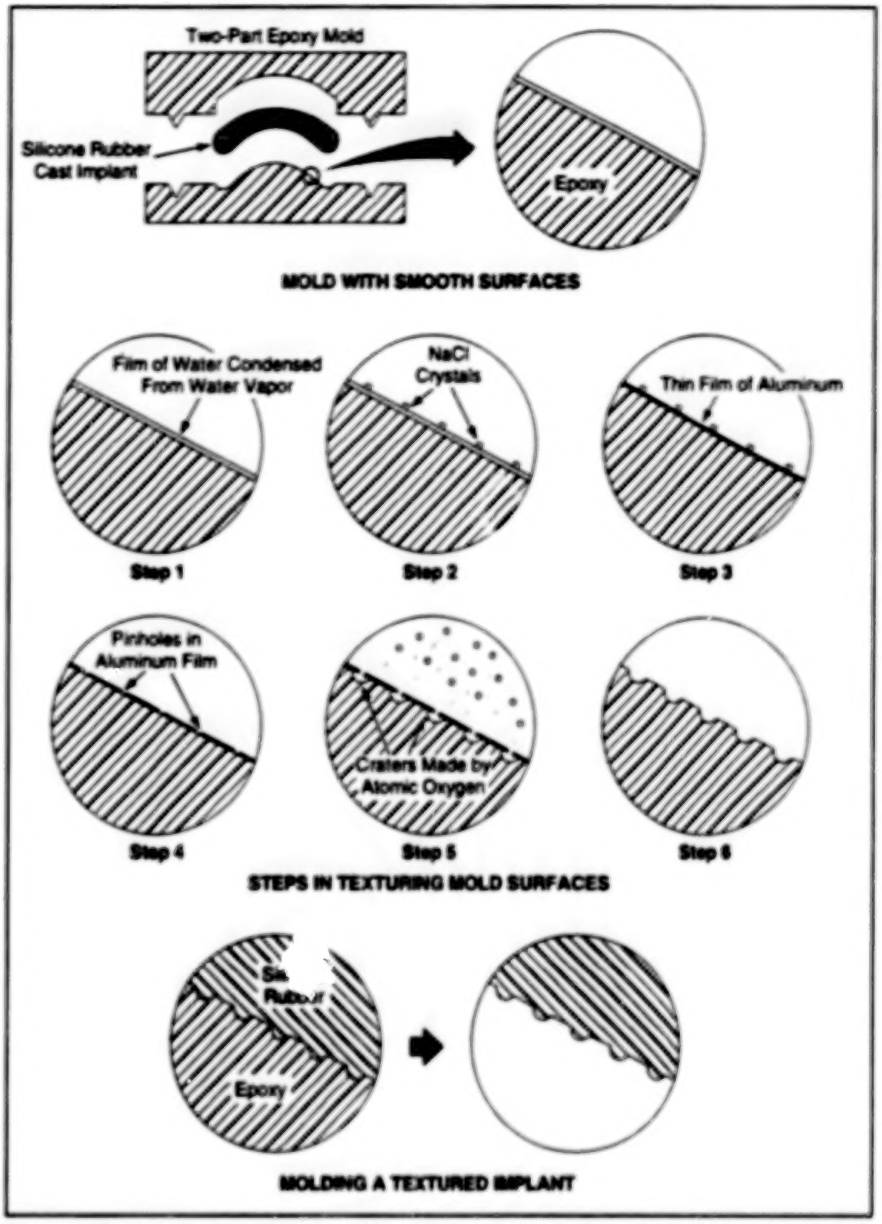

Microscopic Craters are made in the mold surfaces in this sequence of steps. The craters impart microscopic bumps to the cast product.

The mold is then ready for use. Silicone rubber is injected into the mold cavity, where the hemispherical craters impart bumps to the surface of the cast silicone implant. The size and spacing of the mold craters can readily be controlled during fabrication of the mold to produce a cast implant with optimum texture for fixation in the tissue.

This work was done by Bruce A. Banks and Sharon K. Rutledge of **Lewis Research Center**. *Further information is contained in a TSP [see page 1].*

Inquiries concerning rights for the commercial use of this invention should be addressed to the Patent Counsel, Lewis Research Center [see page 1]. Refer to LEW-15805.

Ultralight Thermal Radiator

A modular heat-pipe unit is made of metal foil and polymer sheets.

Lyndon B. Johnson Space Center, Houston, Texas

An ultralightweight heat radiator contains many parallel heat pipes made of laminated sheets of metal and plastic. Versions of the panel can have mass densities between 1.3 and 3.5 kg/m^2 — from one-tenth to one-fourth the densities of previous radiators. The multiple heat pipes provide redundancy and reliability; if one of its pipes fails, the radiator suffers a slight decrease in effective area, not a complete shutdown.

Developed for use in a thermal-control system on a Moon base (see figure), the radiator could be useful on Earth — perhaps as a lightweight, portable heat exchanger for a temporary structure. Water is the working fluid — a suitable nontoxic, nonflammable material for inhabited spaces.

The heat-pipe envelope is a thin, flexible, pressure-tight, heat-sealable laminate. Fabrication is simple: two thin sheets of the laminate are heat-sealed at their edges. The radiator panel can be rolled or folded for transportation to a site, then unfurled for use.

The laminate consists of multiple polymer and metal-foil layers bonded together. The metal foil serves as an impermeable (pressure-sealing) barrier, while the polymer layers support and protect the metal, preventing large local stresses that would open pinholes in the metal foil if the foil were unsupported.

This work was done by Scott D. Garner and Nelson J. Gernert of Thermacore, Inc., for **Johnson Space Center**. *Further information is contained in a TSP [see page 1].*
MSC-22272

The Ultralight Radiator, shown here cooling a habitat on the Moon, would be portable and thus well suited to use at temporary installations on Earth.

Mathematics and Information Sciences

Hardware, Techniques, and Processes

61 Compressing Image Data With Minimal Perceptual Errors

62 Automated Gathering of Information on the Internet

BLANK PAGE

Compressing Image Data With Minimal Perceptual Errors

Invisible or nearly invisible errors are tolerated for the sake of enhanced compression.

Ames Research Center, Moffett Field, California

A computational scheme for reducing the number of bits needed to convey digital imagery is based partly on a concept of management of the quantization errors that increase with increasing degree of compression (decreasing bit rate): one tolerates quantization errors to the extent to which the perceptible degradation of the reconstructed imagery can be eliminated or reduced to an acceptably low level. Thus, in addition to eliminating some redundant image components as do other image-coding schemes, this scheme also eliminates nonredundant invisible image components. The scheme includes an algorithm that optimizes a quantization matrix (which is explained below) in such a way as to yield a reconstructed image with a minimum perceptual error for a given bit rate or a minimum bit rate for a given perceptual error.

The figure illustrates the basic functions of the compression and decompression (reconstruction) aspects of the scheme. A digitized input image is divided into blocks (typically, 8 by 8 pixels each). A discrete cosine transform (DCT) is performed on each block, then the DCT coefficients are quantized. The quantization of each DCT coefficient is determined by an entry in a quantization matrix, which is primarily responsible for the bit rate of transmission and the perceived quality of the reconstructed image. The quantized data can be further compressed before transmission by use of any of a number of established entropy-coding techniques. After reception and decoding, the image data are reconstructed in a process of dequantization (involving multiplication of quantized data by quantization-step sizes), followed by inverse DCT, followed by reassembling the blocks into a complete image.

"Luminance masking" denotes the increases in visual threshold level with increasing local background luminance, while "contrast masking" denotes the decreases in visual thresholds for patterns in the presence of other patterns. In the present scheme, the DCT threshold levels are adjusted for each block to take advantage of luminance- and contrast-masking effects so as to reduce the visible effects of quantization errors. The adjustment is performed by the quantization-matrix-optimizing algorithm, which also pools errors over all blocks in the image and readjusts the quantization matrix for each block to minimize the overall perceptual error.

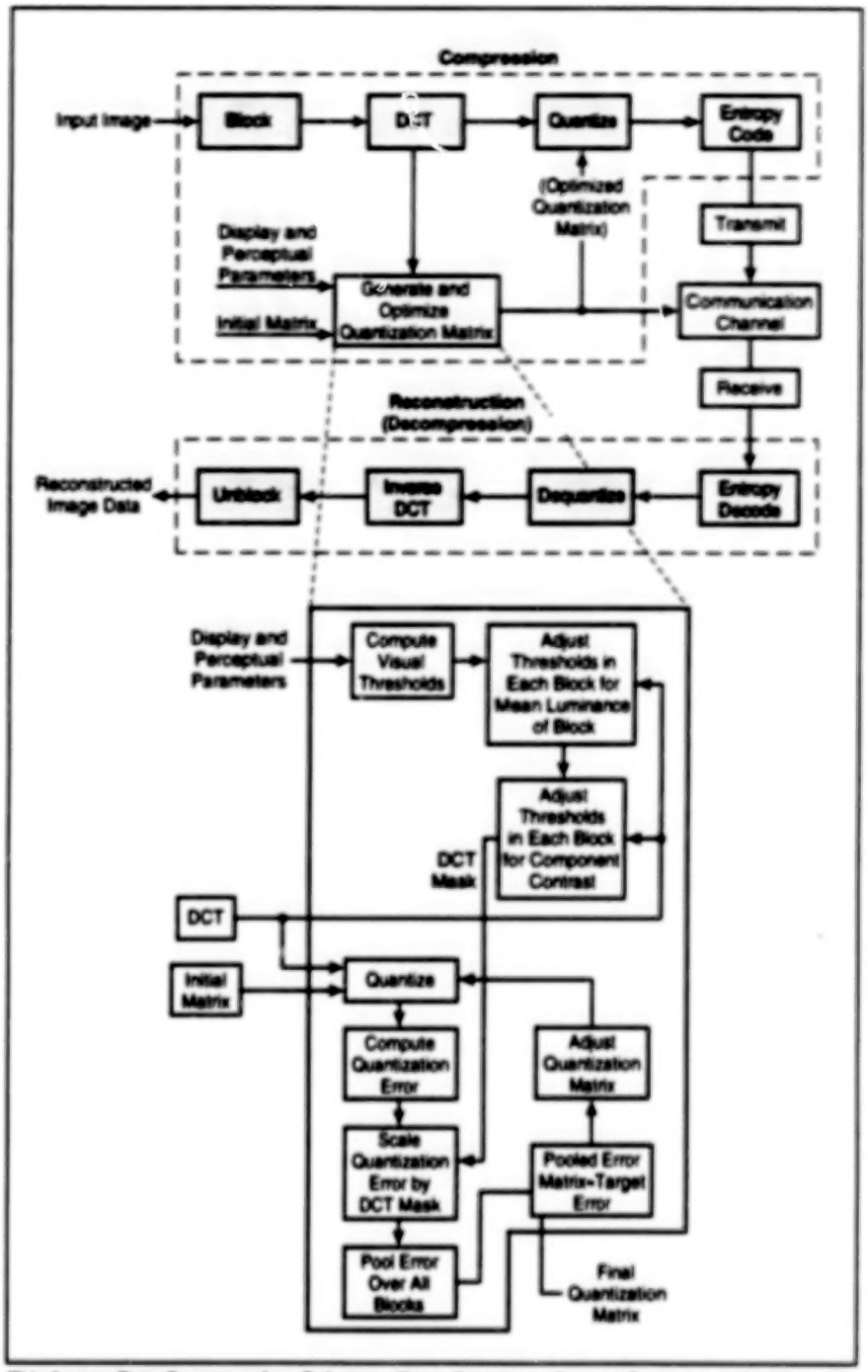

This Image-Data-Compression Scheme utilizes discrete cosine transforms in conjunction with luminance-masking, contrast-masking, error-pooling, and entropy-coding techniques. The scheme includes an optimization algorithm that yields a minimum perceptual error for a given bit rate or a minimum bit rate for a given perceptual error.

This work was done by Andrew B. Watson of **Ames Research Center**. *Further information is contained in a TSP [see page 1].*

This invention has been patented by NASA (U.S. Patent No. 5,426,512). Inquiries concerning nonexclusive or exclusive license for its commercial development should be addressed to the Patent Counsel, Ames Research Center [see page 1]. Refer to ARC-13382.

Automated Gathering of Information on the Internet

A knowledge robot has been designed to serve an educational community.

Lyndon B. Johnson Space Center, Houston, Texas

The Internet Library Information Assembly Database (ILIAD) is a knowledge robot designed primarily to serve primary- and secondary-school educators. "Knowledge robot" denotes one of a number of emerging computer systems that are being developed to help users sift through the vast quantity of information available on the Internet to find the specific information that they need.

As one of these robots, ILIAD is approximately the electronic equivalent of a school librarian with access to a very large collection. The ILIAD helps users retrieve information from the nearly 900 Internet sites that use the Wide Area Information Server (WAIS) communication protocol and the WAIS index structure, which ILIAD classifies by the Dewey Decimal System. Figure 1 indicates the distribution of subject matter in the data bases at the WAIS sites.

The ILIAD is implemented by software that comprises three interacting modules: a subject filter, a preference filter, and controller (see Figure 2). When a user's request is received at the ILIAD site, the subject filter converts the request into a search string. The search string is then matched to applicable classifications in the Dewey Decimal system. Where matches are found, search queries are forwarded to each WAIS site that contains the matching subject matter in its data base. To limit Internet traffic generated by ILIAD, only those ten most suitable responses, which score highest according to a quantitative measure of relevance, are returned over the network.

The preference filter in the ILIAD screens each response to each query according to the previously expressed preferences of individual users or groups of users. The controller and the preference filter accumulate data on preferences as summarized by various quantitative measures of preferability with respect to complexity of text, preferability of images that contain certain characteristic features, and preferability of multimedia presentations (e.g., text and images, text and sound). The output of the preference filter is an ordering of responses according to the probability that the user would choose one over others in the set. Responses found to be unsuitable according to the quantitative measures of preference are discarded, while the suitable responses are sent to the user.

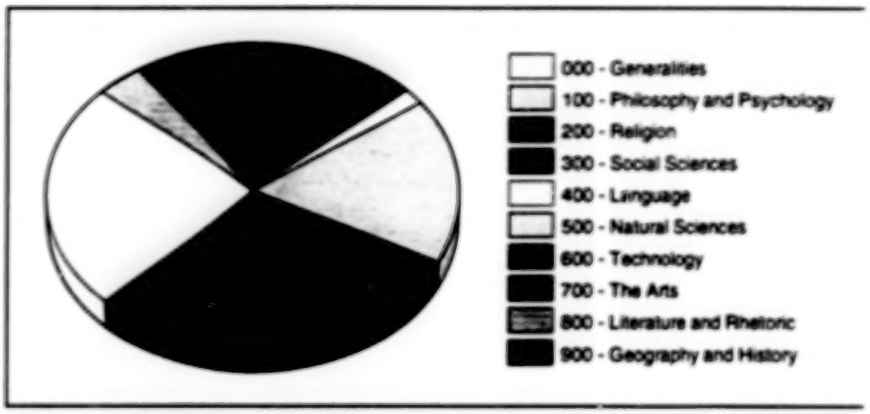

Figure 1. The Distribution of Information stored in the WAIS data bases is shown in Dewey decimal classifications. The largest segment, Generalities, includes material on computer science, software, and related methods.

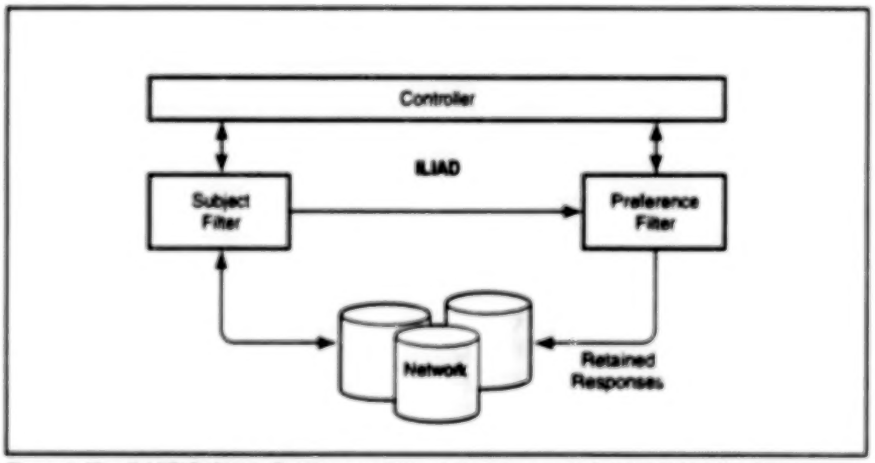

Figure 2. The ILIAD Software System comprises interacting modules that search for data according to the quantitative measures of (a) relevance of subject matter to each query and (b) accumulated data on users' preferences.

This work was done by Mark E. Ponvig and Robert O. Shelton of **Johnson Space Center**. *Further information is contained in a TSP [see page 1].*

MSC-22551

END

11-26-97